# High-Intensity Interval Training Remodels the Proteome and Acetylome of Human Skeletal Muscle

Hostrup M[1+*], Lemminger AK[1+], Stocks B[2+], Gonzalez-Franquesa A[2], Larsen JK[2], Prats Quesada J[2], Thomassen M[1], Weinert BT[3], Bangsbo J[1], & Deshmukh AS[2,4*]

[1]Section of Integrative Physiology, Department of Nutrition, Exercise and Sports, University of Copenhagen, Copenhagen, Denmark

[2]Novo Nordisk Foundation Center for Basic Metabolic Research, Faculty of Health and Medical Sciences, University of Copenhagen, Copenhagen, Denmark

[3]The Novo Nordisk Foundation Center for Biosustainability, Technical University of Denmark, Copenhagen, Denmark.

[4]The Novo Nordisk Foundation Center for Protein Research, Clinical Proteomics, Faculty of Health and Medical Sciences, University of Copenhagen, Copenhagen, Denmark.

**[+]Joint first-authors**

***Corresponding authors:**

**Atul S Deshmukh (Lead contact)**

Novo Nordisk Foundation Center for Basic Metabolic Research, Faculty of Health and Medical Sciences, University of Copenhagen, Blegdamsvej 3B, DK2200, Copenhagen, Denmark

Phone: +45 35 32 53 13; e-mail: atul.deshmukh@sund.ku.dk

**Morten Hostrup**

Section of Integrative Physiology, Department of Nutrition, Exercise and Sports, University of Copenhagen, 13, Universitetsparken, DK 2100, Denmark

Phone: +45 24 47 47 85; e-mail: mhostrup@nexs.ku.dk

## Abstract

Exercise is an effective strategy in the prevention and treatment of metabolic diseases. Alterations in the skeletal muscle proteome, including post-translational modifications, regulate its metabolic adaptations to exercise. Here, we examined the effect of high-intensity interval training (HIIT) on the proteome and acetylome of human skeletal muscle, revealing the response of 3168 proteins and 1263 lysine acetyl-sites on 464 acetylated proteins. We identified global protein adaptations to exercise training involved in metabolism, excitation-contraction coupling, and myofibrillar calcium sensitivity. Furthermore, HIIT increased the acetylation of mitochondrial proteins, particularly those of complex V. We also highlight the regulation of exercise-responsive histone acetyl-sites. These data demonstrate the plasticity of the skeletal muscle proteome and acetylome, providing insight into the regulation of contractile, metabolic and transcriptional processes within skeletal muscle. Herein, we provide a substantial hypothesis-generating resource to stimulate further mechanistic research investigating how exercise improves metabolic health.

## Impact statement

Hostrup and colleagues identify global proteomic and acetylomic adaptations to high-intensity interval training, demonstrating adaptations to processes regulating metabolism and contraction.

## Introduction

Exercise training is the most effective means to improve cardiovascular fitness and metabolic health, both being predominant determinants of life expectancy and all-cause mortality (Mandsager et al., 2018). Alterations to the proteome of skeletal muscle underpin its adaptations to exercise training, including glucose and fatty acid metabolism, insulin sensitivity, mitochondrial respiration, immune function and excitation-contraction coupling (Deshmukh et al., 2021; Egan & Zierath, 2013; Gonzalez-Franquesa et al., 2021; Holloway et al., 2009; Morten Hostrup & Bangsbo, 2017; Robinson et al., 2017; Ubaida-Mohien et al., 2019). Furthermore, proteome-wide post-translational modifications play an important role in regulating metabolism via modulating signaling, protein stability and enzyme activity (Baeza, Smallegan, & Denu, 2016; Cohen, 2000), and are sensitive to exercise stimuli (Hoffman et al., 2015; Overmyer et al., 2015; Parker, Kiens, Wojtaszewski, Richter, & James, 2020).

The application of mass-spectrometry-based proteomics has vastly expanded the catalog of post-translationally modified proteins, and in doing so has revealed novel insights into both histone and non-histone acetylation (Choudhary, Weinert, Nishida, Verdin, & Mann, 2014; Hansen et al., 2019; Narita, Weinert, & Choudhary, 2019; Svinkina et al., 2015). Nevertheless, the understanding of the acetylome in human skeletal muscle is still incomplete and remains to be studied in response to exercise training. Numerous cellular processes are regulated by protein acetylation, including transcription, metabolism, apoptosis, growth and muscle contraction among others (Narita et al., 2019). Lysine acetylation is an evolutionarily conserved post-translational modification, whereby lysine acetyltransferases catalyze the transfer of an acetyl group from acetyl-CoA to the ε-amino acid side chain of lysine and deacetylases remove acetyl groups from lysine residues. Alternatively, acetyl groups can be non-enzymatically transferred to lysine from acetyl-CoA (Hansen et al., 2019; James,

Smith, Smith, Robinson, & Murphy, 2018; Pougovkina et al., 2014; Weinert, Moustafa, Iesmantavicius, Zechner, & Choudhary, 2015). In human *vastus lateralis* muscle biopsies from male athletes, 941 acetylated proteins containing 2811 lysine acetylation sites have been identified (Lundby et al., 2012). Mitochondria were the cellular component of human skeletal muscle exhibiting the greatest proportion of acetylated proteins (Lundby et al., 2012). Furthermore, the sensitivity of the acetylome to physiological stimuli has been demonstrated in rodents in response to acute fasting and chronic caloric restriction in liver (Hebert et al., 2013; Pougovkina et al., 2014; Weinert et al., 2015) as well as acute exercise (Overmyer et al., 2015) and high-fat diet (Williams et al., 2020) in skeletal muscle (Overmyer et al., 2015).

Continual advances in mass spectrometry-based proteomic technologies and approaches are increasing the depth and coverage of proteomic analyses. Nevertheless, proteome and proteome-wide post-translational modification analyses of skeletal muscle tissue remain highly challenging due to a wide dynamic range of protein abundances (Deshmukh et al., 2015). Single-shot data-dependent acquisition (DDA) analyses are often limited in their protein identifications and are characterized by relatively poor data completeness (i.e. high number of missing values) (Tabb et al., 2010). However, the relatively recent development of data-independent acquisition (DIA) is helping to vastly reduce the proportion of missing data while simultaneously improving proteome depth in single-shot analyses of complex tissues (Ludwig et al., 2018). Nonetheless, DDA in combination with peptide-level fractionation remains a useful approach to overcome sample complexity, particularly when performing post-translational modification proteomics.

In this study, untrained men undertook five weeks of high-intensity interval training (HIIT) and *vastus lateralis* muscle biopsies were collected before and after HIIT for proteomic and lysine-acetylome

88 analyses. We investigated the adaptation to HIIT in a deep human skeletal muscle proteome and
89 undertook the first investigation of the acetylomic adaptations to exercise training within human
90 skeletal muscle. HIIT remodeled skeletal muscle favoring mitochondrial biogenesis, but induced
91 changes in protein abundance indicative of reduced calcium sensitivity. Furthermore, HIIT increased
92 acetylation, particularly of the mitochondria and enzymes of the tricarboxylic acid (TCA) cycle.
93

94 **Results and Discussion**

95 **Physiological adaptations to HIIT**

96 Eight untrained men (23–38 years of age; Figure 1-figure supplement 1) completed a HIIT regimen
97 (Figure 1A) that consisted of five weeks of supervised cycling, performed as 4 – 5 × 4-min intervals
98 at a target heart rate of >90%-max interspersed by 2 mins of active recovery, undertaken three times
99 weekly. Participants were healthy, non-smokers and occasionally active, but otherwise untrained.
100 Characteristics of the participants are presented in Figure 1B. Participants experienced a 14% and
101 17% improvement in maximal oxygen consumption ($\dot{V}O_{2max}$) and incremental peak power output,
102 respectively, during HIIT (Figure 1B and C; $p < 0.001$), which compares favorably to typical HIIT-
103 induced adaptations (Wen et al., 2019). In addition, participants gained an average of 1.0 ± 0.3 kg
104 lean mass during HIIT training, without changes in fat mass (Figure 1B). The rate of fat oxidation
105 during submaximal cycling (50-150 W) increased following HIIT (Figure 1D), while no apparent
106 changes were observed for carbohydrate oxidation (Figure 1E).
107

108 **HIIT increases mitochondrial respiratory capacity of skeletal muscle**

109 Resting muscle biopsies were collected from the *vastus lateralis* before and three days after the final
110 training session. Mitochondrial respirometry analyses were immediately performed on the freshly
111 excised muscle samples using a substrate-uncoupler-inhibitor titration protocol (Pesta et al., 2011) on

112 a high-resolution O2K respirometer (Oroboros, Innsbruck, Austria). In line with previous findings
113 (Christensen et al., 2016; Dohlmann, Hindsø, Dela, Helge, & Larsen, 2018; Granata, Oliveira, Little,
114 Renner, & Bishop, 2016; Jacobs et al., 2013; Larsen et al., 2015; Meinild Lundby et al., 2018), HIIT
115 increased mitochondrial respiration across a range of respiratory states, increasing CI+II coupled
116 respiration by 30% ($p < 0.001$) and electron transport system capacity by 15% ($p = 0.049$) (Figure
117 1F). Furthermore, HIIT induced a robust increase in citrate synthase activity by 42% ($p = 0.002$)
118 (Figure 1G), a validated marker of mitochondrial volume in human skeletal muscle (Larsen et al.,
119 2012).
120

121 **Elevated mitochondrial respiration is underpinned by increased abundance of mitochondrial**
122 **proteins following HIIT**

123 Skeletal muscle biopsy samples were prepared for liquid-chromatography tandem mass spectrometry
124 and measured using single-shot DIA (Ludwig et al., 2018) (Figure 1H). We obtained extensive
125 proteome coverage identifying 3343 proteins (Supplementary File 1). After applying a filter of 4 valid
126 values out of the 8 participants in at least one time point, 3168 proteins were quantified within skeletal
127 muscle (Supplementary File 2). Due to the nature of DIA, few missing values required imputation in
128 each sample (Figure 1-figure supplement 2A; mean proteins quantified per sample: 2853 ± 33). Good
129 correlation (median correlation: 0.88) between biological replicates (participants at the same time
130 point) was apparent (Figure 1-figure supplement 2B). Furthermore, the proteome contained good
131 coverage across multiple cellular compartments (Figure 1-figure supplement 2C). Principal
132 component analysis demonstrated inter-sample variation, however samples did cluster by time point
133 (Figure 1-figure supplement 2D). Overall, our DIA proteome analysis displayed extensive coverage,
134 demonstrated by the quantification of low abundant proteins such as transcription factors (e.g.
135 CREB1 and TFEB) and myokines (e.g. IL18; Supplementary File 1).

136

137 HIIT regulated 126 proteins (permutation-based FDR<0.05). Of these, 102 proteins were upregulated,
138 while 24 were downregulated (Figure 2A, Supplementary File 2). These included the upregulation of
139 classical endurance exercise training-responsive mitochondrial proteins (e.g. cytochrome c oxidase
140 subunit 5b; COX5B & NADH dehydrogenase 1 alpha subcomplex subunit 7; NDUFA7), as well as
141 proteins involved in $NAD^+$ metabolism (e.g. nicotinamide phosphoribosyltransferase; NAMPT),
142 branched-chain amino acid metabolism (branched-chain alpha-ketoacid dehydrogenase kinase;
143 BCKDK) and ubiquinone biosynthesis (5-demethoxyubiquinone hydroxylase; COQ7), the latter of
144 which we have recently described in exercise-trained mouse skeletal muscle (Gonzalez-Franquesa et
145 al., 2021) (Figure 2A). We also identified novel exercise-training regulated proteins, including, but
146 not limited to, glutaminyl-tRNA synthase (QARS) and rab GDP dissociation inhibitor alpha (GDI1).
147 QARS, which catalyzes the glutamate aminoacylation of tRNA and thus plays a central role in
148 translation (Deutscher, 1984), was amongst the most significantly upregulated proteins within the
149 proteome. In addition, GDI1, which inhibits insulin-stimulated glucose uptake by preventing the
150 dissociation of GDP from Rab10 (Y. Chen et al., 2009), was lowered, providing a novel potential
151 mechanism for the insulin-sensitizing effects of exercise training.

152

153 After filtering for differentially regulated proteins, enrichment analysis using Fisher's exact test
154 indicated the predominant regulation of mitochondrial proteins (e.g. GOCC: mitochondrial part and
155 mitochondrial inner membrane) (Figure 2B, Supplementary File 3). Hierarchical clustering analysis
156 on z-scored differentially regulated proteins identified that the mitochondrial terms were enriched
157 within the upregulated proteins (Figure 2C). Summed protein abundances also demonstrated
158 mitochondrial biogenesis (Figure 2D), including upregulated protein content of electron transport
159 chain complexes (Figure 2E and Figure 2-figure supplement 1), mitochondrially-encoded proteins

160 (Figure 2F) and proteins containing a mitochondria-targeting transit peptide (Figure 2G). Thus, the
161 increase in the proteome mirrors the functional increase in mitochondrial respiratory capacity of
162 skeletal muscle after HIIT (Figure 1F).
163

164 **HIIT regulates proteins involved in skeletal muscle excitation-contraction coupling**

165 We next investigated whether HIIT influenced the fiber-type proportions of skeletal muscle. While
166 HIIT did not change skeletal muscle fiber-type composition in terms of myosin heavy chain isoforms
167 (Figure 3A) and myosin light chain proteins (Figure 3B), a coordinated regulation of proteins
168 modulating myosin light chain phosphorylation was identified (Figure 3C). Abundance of myosin
169 light chain kinase 2 (MYLK2) decreased concomitantly with a reduction in smoothelin-like protein
170 1 (SMTNL1), an inhibitor of the myosin phosphatase complex (Wooldridge et al., 2008) and an
171 increase in myosin phosphatase-targeting subunit 1 (PPP1R12A), the myosin-targeting regulatory
172 subunit of protein phosphatase 1 (Alessi, MacDougall, Sola, Ikebe, & Cohen, 1992) (Figure 3C).
173 Reduced MYLK2 abundance was confirmed by immunoblotting (Figure 3-figure supplement 1A).
174 Furthermore, we have previously detected these adaptations in slow- and fast-twitch muscle fibers
175 following moderate-intensity continuous cycling training (Deshmukh et al., 2021). Given that
176 phosphorylation of myosin light chains promotes myofibrillar calcium sensitivity (Davis et al., 2001),
177 the reduction in both MYLK2 and SMTNL1 alongside an increase in PPP1R12A indicates an
178 adaptation towards reduced myosin phosphorylation and lowered calcium sensitivity following
179 exercise training. Indeed, myofibrillar calcium sensitivity decreases following high-intensity sprint
180 training in untrained males, particularly at a low pH representing physiological exercising conditions
181 (Lynch, McKenna, & Williams, 1994). Although the functional importance of such adaptations
182 remains elusive, knockdown of Smtnl1 augments exercise training-induced improvements in
183 endurance performance, while sedentary Smtnl1$^{-/-}$ mice display a fiber-type switch mimicking

184 endurance exercise training (Wooldridge et al., 2008). While we did not observe any concomitant
185 myosin fiber-type switching (Figure 3A), the changes observed in proteins regulating myosin
186 phosphorylation following HIIT could result in a right-shift of the $Ca^{2+}$-force relationship, meaning
187 that a higher myoplasmic calcium concentration would be required for a given force production. This
188 decline in myofibrillar calcium sensitivity may, however, support faster off-kinetics of calcium from
189 troponin-C to be re-sequestered in the sarcoplasmic reticulum. Therefore, the changes observed in
190 proteins regulating myosin phosphorylation following HIIT provide an intriguing mechanism for a
191 HIIT-induced reduction in calcium sensitivity and warrants further attention.
192
193 Providing a further link to the altered calcium handling following HIIT (Lynch et al., 1994), we
194 identified a downregulation of L-type calcium channel subunits, otherwise known as the
195 dihydropyridine receptor (DHPR) (Figs. 3 D and E). DHPR controls the coupling of membrane
196 depolarization and sarcoplasmic reticulum $Ca^{2+}$-release in skeletal muscle via its interaction with
197 ryanodine receptor 1 (RYR1) (Flucher & Franzini-Armstrong, 1996). Conversely to DHPR, HIIT did
198 not influence the abundance of RYR1 (Figure 3F) or the sarcoplasmic/endoplasmic reticulum calcium
199 ATPases 1-3 (ATP2A1-3 (SERCAs); Figure 3-figure supplement 1B). The observation that DHPR
200 abundance declined following HIIT points to a 'slowing' of muscle fibers. Indeed, a period of training
201 can induce rapid changes in the abundance of proteins with importance for calcium handling,
202 irrespective of changes in fiber type distribution (M. Hostrup et al., 2019; M. Hostrup, Onslev,
203 Jacobson, Wilson, & Bangsbo, 2018; Majerczak, Karasinski, & Zoladz, 2008; Munkvik et al., 2010;
204 Ortenblad, Lunde, Levin, Andersen, & Pedersen, 2000). Fast-twitch fibers have greater sarcoplasmic
205 reticulum volume, faster calcium release and re-uptake kinetics, and a greater content of DHPR than
206 slow-twitch fibers (Banas, Clow, Jasmin, & Renaud, 2011; Deshmukh et al., 2021; Murgia et al.,

207 2017). Thus, the HIIT-induced reduction of DHPR abundance may represent a slowing of muscle
208 fibers independently of their myosin heavy chain abundance.
209
210 **Lysine acetylomics of skeletal muscle identifies the predominant acetylation of mitochondrial**
211 **and acetyl-coA metabolic proteins**
212 Skeletal muscle biopsy samples were prepared for lysine acetylomics using a PTMscan Acetyl-Lysine
213 Motif kit (Cell Signaling Technology) (Svinkina et al., 2015) and measured via liquid-
214 chromatography tandem mass spectrometry using DDA. Due to limited sample availability from one
215 participant, lysine acetylomics was performed for 7 of the participants. We identified a total of 1990
216 acetyl-sites on 664 proteins (Supplementary File 4). While this is fewer than the 2811 acetyl-sites on
217 941 proteins identified in the largest human skeletal muscle acetylome to date (Lundby et al., 2012),
218 we identified 1073 acetyl-sites that were not identified in the analysis of Lundby et al (Figure 4-figure
219 supplement 1A). The difference in acetyl-sites identified between the two studies likely reflects a
220 combination of exercise-induced acetylation revealing novel-acetyl sites, and the stochastic nature of
221 data-dependent acquisition, the different LC-MS/MS instruments employed, and the use of updated
222 FASTA files. Nonetheless, we substantially extend the human skeletal muscle acetylome. After
223 applying a filter of 4 valid values out of the 7 participants in at least one time point we quantified
224 1263 acetylated sites on 464 proteins within skeletal muscle (Figs. 1G & 4A, Supplementary File 5).
225 Six and 42 acetyl-sites were quantified exclusively in the pre- and post-HIIT samples, respectively.
226 The mean number of acetyl-sites quantified in each sample was 976 (Figure 4-figure supplement 1B).
227 Median correlation between biological replicates (between participants at the same time point) was
228 0.76 (Figure 4-figure supplement 1C), indicating greater variation in the human acetylome than the
229 proteome, as would be expected (Lundby et al., 2012). The acetylome also displayed extensive
230 coverage across multiple cellular compartments (Figure 4-figure supplement 1D), which largely

231 reflected the abundance distribution of the proteome (Figure 1-figure supplement 2C), albeit with a
232 slight relative increase in the mitochondrial identifications. Principal component analysis identified
233 variation in the acetylome between samples (Figure 4-figure supplement 1E). Although there was no
234 clear separation of samples by time point, a leftward shift is apparent on component 1 from pre to
235 post samples for almost all participants (six out of seven). There was considerable overlap with
236 proteins quantified in the proteome, with 421 proteins quantified in both (Figure 4A). Of the
237 quantified acetylated sites (1263), the majority (1232) were located on these 421 proteins (Figure
238 4A). Single acetyl-sites were quantified on the majority of proteins, with a trend for decreasing
239 frequency with additional acetyl-sites (Figure 4B). However, several proteins were quantified with a
240 large number of acetylation sites (e.g. ≥ 15 acetyl-sites) (Figure 4B), examples of which include the
241 contractile proteins titin (TTN) and slow-twitch myosin beta (MYH7).
242
243 After summing the median intensities of acetyl peptides from each protein in the pre-HIIT samples,
244 we ranked the abundance of acetylated proteins within skeletal muscle (Supplementary File 6) and
245 highlighted the top 10 proteins with the highest acetyl-intensity (Figure 4C). Histone H4 (HIST1H4A)
246 had the highest acetylation intensity, making up approximately 10% of the total acetylome intensity,
247 supporting the regulatory role of histone acetylation in modulating transcription (Sterner & Berger,
248 2000; Strahl & Allis, 2000). The majority of the remaining top acetylated proteins were metabolic
249 enzymes, including the TCA cycle proteins malate dehydrogenase (MDH2) and fumarate hydratase
250 (FH), as well as subunits of complex V (ATP5H and ATP5O) within the electron transport chain.
251 Superoxide dismutase (SOD2), a canonical acetylated enzyme involved in mitochondrial reactive
252 oxygen species handling (St Clair, Wan, Oberley, Muse, & St Clair, 1992; Z. Tao, Gao, & Liu, 2009),
253 also displayed high acetylation intensity. We further compared the protein abundance rank for these
254 high-intensity acetylated proteins within the proteome (Figure 4D). These proteins did not appear to

255 be the highest intensity acetylated proteins simply due to their relative protein abundance. While they
256 all fell within the top 318 proteins in the proteome, they did not make up the most abundant proteins,
257 except for creatine kinase M-type (CKM), which is extremely abundant in skeletal muscle (Figure
258 4D). To identify systematic trends in protein acetylation, we performed a one-dimensional enrichment
259 analysis (Juergen Cox & Mann, 2012) on the summed protein acetylation intensities, which ranked
260 the proteins by acetylation intensity and identifies Gene Ontology (GO) annotations that are
261 systematically over-represented with higher intensities (positive enrichment factor) and lower
262 intensities (negative enrichment factor). This identified mitochondrial terms (e.g. GOCC:
263 mitochondrial part and mitochondrial matrix) as enriched for high acetylation intensity (Figure 4E
264 and Supplementary File 7). In particular, proteins of carboxylic acid metabolic processes (e.g. TCA
265 cycle) and monovalent inorganic cation transport (e.g. electron transport chain complex V proteins)
266 display systematically high acetylation intensity (Figure4E and Supplementary File 7). Furthermore,
267 the Uniprot keyword term "muscle protein" was also enriched for high acetylation intensity, a term
268 that mainly encompasses the contractile machinery of skeletal muscle (e.g. myosins).
269
270 In order to examine acetylation stoichiometry within skeletal muscle, we estimated the relative
271 stoichiometries of acetyl-sites using abundance-corrected intensities (ACI) (Supplementary File 8).
272 ACIs were calculated by dividing acetyl-peptide intensities by the intensities of their corresponding
273 protein, with ACI values correlating with stoichiometry (Hansen et al., 2019). After ranking acetyl-
274 site ACI for the pre-HIIT samples, we highlighted the top 10 acetyl-sites with the highest ACI (Figure
275 4F). Trifunctional enzyme subunit alpha (HADHA), FH, HIST1H4A and 3- ketoacyl-CoA thiolase
276 (ACAA2), which were identified as among the highest intensity acetylated proteins (Figure 4C), all
277 contain high stoichiometry acetyl-sites (Figure 4F). However, nicotinamide nucleotide
278 transhydrogenase (NNT) K70 had the highest ACI within skeletal muscle (Figure 4F). NNT is an

279 inner mitochondrial membrane protein, which uses the proton motive force to maintain high levels
280 of NADPH (Hoek & Rydström, 1988) and in doing so can regulate metabolism (Freeman, Hugill,
281 Dear, Ashcroft, & Cox, 2006; Ho, Lin, Lin, Wu, & Cheng, 2017). NNT is also highly acetylated in
282 cardiac muscle (Foster et al., 2013), although the effect of acetylation on NNT activity remains to be
283 determined. Nonetheless, NNT can regulate acetylation via NADPH-mediated regulation of histone
284 deacetylase 1 (HDAC1) activity (Ho et al., 2017), thus acetylation of NNT may represent a feedback
285 mechanism controlling cellular acetylation and metabolism.
286
287 To identify systematic trends in acetyl-site stoichiometry, we performed a one-dimensional
288 enrichment analysis (Juergen Cox & Mann, 2012) on acetyl-site ACI using the leading protein ID for
289 relative enrichment (Tyanova et al., 2016). We identified the mitochondria (e.g. GOCC:
290 mitochondrial part and mitochondrial inner membrane) and carboxylic acid catabolic processes to be
291 enriched within higher stoichiometry acetylated proteins (Figs. 4G, 4H & Supplementary File 9). This
292 extends previous analyses by not only showing that mitochondrial proteins make up the majority of
293 acetylated proteins in skeletal muscle (Lundby et al., 2012), but also by identifying mitochondrial
294 proteins as having relatively high stoichiometry acetyl-sites – an observation that is consistent with
295 analyses in HeLa cells, rodent liver and yeast (Hansen et al., 2019; Weinert et al., 2014; Weinert et
296 al., 2015). Enriched for proteins with low stoichiometry acetyl-sites were proteins involved in
297 contraction (e.g. GOCC: contractile fiber part; Figs. 4G, 4H & Supplementary File 9), including the
298 Uniprot keyword term "muscle protein" (Figure 4G), which, conversely, was enriched for high
299 protein acetylation intensity (Figure 4E). Myosin displayed the greatest enrichment for low
300 acetylation stoichiometry (Figure 4G). Thus, despite contractile proteins displaying high protein
301 acetylation intensity and making up a substantial number of known acetylated proteins within skeletal
302 muscle (Lundby et al., 2012), they contain acetylation sites of relatively low stoichiometry. The high

303 acetylation intensity of these proteins is therefore likely due to high protein abundance and a large
304 number of acetylation sites per protein. Proteins annotated to the cytosol and plasma membrane also
305 displayed low acetyl-site ACI (Figure 4G). This highlights differences in the inter-organelle
306 acetylation levels of skeletal muscle and can likely be explained by subcellular compartmentalization
307 of acetyl-CoA (Pietrocola, Galluzzi, Bravo-San Pedro, Madeo, & Kroemer, 2015).
308

309 **HIIT induces acetylation of mitochondrial and TCA cycle proteins**

310 HIIT increased the mean number of acetyl-sites quantified per sample by over 100 sites (Pre: 915 ±
311 44, Post: 1037 ± 51; $p = 0.015$; Figure 4-figure supplement 1B). Using a stringent statistical approach
312 of permutation-based FDR corrected paired t-tests, we identified 20 upregulated acetyl-sites and 1
313 downregulated site (FDR < 0.05; Figure 5A). In addition, by applying a validated, albeit less stringent,
314 significance score (Π-value), which combines the statistical significance (p-value) with the fold
315 change (Xiao et al., 2014), we extended this to identify 257 upregulated and 26 downregulated acetyl-
316 sites following HIIT (Π < 0.05; Figure 5A and Supplementary File 5). In general, there was a trend
317 for increased acetylation following HIIT (Figure 5A), which could not be explained by changes in
318 protein content as the fold changes in acetylation generally exceeded those of protein abundance
319 (Figure 5B). Therefore, we did not normalize the acetylome data to protein abundance. The increase
320 in protein acetylation was subsequently validated via immunoblotting (Fig 5-figure supplement 1).
321 Within the increased sites, acetyl-sites on metabolic enzymes isocitrate dehydrogenase (IDH2),
322 pyruvate dehydrogenase E1 component subunit alpha (PDH1A), succinate CoA ligase subunit alpha
323 (SUCLG1) and ATP synthase coupling factor 6 (ATP5J) were apparent (Figure 5A), while
324 hyperacetylation of SOD2 occurred at K68, 75, 122 and 130 in response to HIIT (Figure 5A).
325 Included within the downregulated sites were acetyl-sites on annexin A6 (ANXA6), laminin (LMNA)
326 and p38 mitogen-activated protein kinase γ (MAPK12) (Figure 5A). Interestingly, Histone H1.5

327 (HIST1H1B) K48 showed increased acetylation, despite significantly reduced protein abundance
328 (Figure 5B).
329
330 A Fisher's exact test of HIIT-regulated acetyl-sites ($\Pi < 0.05$), using leading protein ID for relative
331 enrichment, indicated the predominant regulation of the TCA cycle pathway, mitochondrial proteins
332 (e.g. GOCC: mitochondrial part and mitochondrial inner membrane) and, in particular, electron
333 transport chain complex V proteins (GOCC: mitochondrial proton-transporting ATP synthase
334 complex) (Figure 5C, Supplementary File 10). These GO terms were strikingly similar to the terms
335 enriched for high acetylation intensity and stoichiometry in the pre-HIIT samples (Figs. 4E and G),
336 indicating that proteins that are highly acetylated in the basal state are most susceptible to increased
337 acetylation following HIIT. To further explore the regulation of HIIT-induced acetylation in skeletal
338 muscle, we looked for consensus sequences around the acetylated lysine residues using iceLogo
339 (Colaert, Helsens, Martens, Vandekerckhove, & Gevaert, 2009). We identified a sequence with a
340 predominance of proximal cysteine residues as well as an aspartic acid residue in the +1 position
341 (Figure 5D). The aspartic acid at +1 is a feature of mitochondrial acetylated proteins (Lundby et al.,
342 2012) and its enrichment is likely due to the over-representation of mitochondrial proteins in the
343 upregulated acetyl-sites (Figure 5C). Proximal cysteine residues are associated with promoting non-
344 enzymatic lysine acetylation (Hansen et al., 2019; James et al., 2018) via initial cysteine acetylation
345 followed by transfer of the acetyl group to lysine (James et al., 2018). Indeed, non-enzymatic
346 acetylation increases alongside elevated fatty acid oxidation (Pougovkina et al., 2014), as is apparent
347 in skeletal muscle mitochondria after HIIT (Figs. 1E). This likely occurs through changes in acetyl-
348 CoA concentration and/or increased acetyl-CoA flux (Pougovkina et al., 2014). Although acetyl-CoA
349 content within resting skeletal muscle does not change in response to exercise training (Putman et al.,
350 1998), acetyl-CoA levels and TCA cycle flux increase during exercise (Constantin-Teodosiu, Carlin,

351 Cederblad, Harrist, & Hultman, 1991; Gibala, MacLean, Graham, & Saltin, 1998; Howlett et al.,
352 1998; Putman et al., 1998), which may result in an accumulation of lysine acetylation during repeated
353 bouts of exercise. Conversely, acute exercise decreases skeletal muscle acetylation in exercising rats
354 (Overmyer et al., 2015), but whether this is the case for humans remains to be determined.
355 Nonetheless, we identify a robust increase in skeletal muscle acetylation, predominantly of
356 mitochondrial proteins, following five weeks of HIIT in humans.
357
358 Because HIIT altered the skeletal muscle acetylome, we examined proteins regulating acetylation in
359 skeletal muscle. A subset of sirtuins (SIRT2, SIRT3, and SIRT5), a family of protein deacetylases,
360 were quantified in the proteome. SIRT3, a mitochondrial-localized deacetylase, displayed a small but
361 non-significant trend for increased abundance following exercise training (Supplementary File 2). To
362 further investigate this, we immunoblotted for SIRT1, SIRT3, SIRT5 and SIRT6. Of the cystosolic
363 and nuclear-localized SIRTs, the abundance of SIRT1 did not change, while SIRT6 increased by
364 27%. The mitochondrial-localized SIRT3 and SIRT5 increased in abundance by 61% and 32%,
365 respectively, following HIIT (Figure 5E). Thus, mitochondrial acetylation increased concomitantly
366 with an increase in the abundance of mitochondrial sirtuins (Figs. 5B and 5E). Conversely, the protein
367 abundance of the mitochondrial acetyltransferase general control of amino acid synthesis 5 like-1
368 (GCN5L1) was unchanged by exercise training (Fig 5E). Although the deacetylase activity of SIRT5
369 has been questioned, instead displaying a preference for desuccinylase and demalyonylase activity
370 (Du et al., 2011; Peng et al., 2011), SIRT3 appears to play a major role in suppressing non-enzymatic
371 mitochondrial acetylation (Weinert et al., 2015). Therefore, elevated SIRT3 abundance following
372 exercise training might be interpreted as a mechanism to suppress excess acetylation, either to
373 preserve the activity of mitochondrial enzymes (Hirschey et al., 2010; R. Tao et al., 2010;

374 Vassilopoulos et al., 2014) or to scavenge acetyl groups for reintegration into acetyl-CoA and energy
375 production.
376
377 Given the enrichment of mitochondrial terms and particularly of complex V proteins in the HIIT-
378 regulated acetylated proteins, we filtered for proteins annotated to the different complexes of the
379 electron transport chain using the HUGO database (Braschi et al., 2019) and highlighted the
380 regulation of each acetyl-site on these proteins alongside the changes in protein abundance (Figure
381 6A). While proteins of complexes I, II, III and IV showed a mixed acetylation response to exercise
382 training, almost every quantified complex V protein had at least one acetyl-site that increased
383 following HIIT (Figure 6A). In fact, ATPase inhibitor (ATPIF1), one of the two complex V proteins
384 that do not show elevated acetylation, is a negative regulator of complex V and is unlikely to be
385 constitutively bound to the ATP synthase complex (Campanella et al., 2008). Why complex V
386 displays elevated acetylation levels both in the basal (Figure 4E) and exercise trained states is unclear
387 (Figs. 5C and 6A). However, as a large proportion of ATP synthase extends into the mitochondrial
388 matrix, many subunits are likely to be more exposed to acetyl-CoA than other membrane-embedded
389 electron transport chain complexes. In support, we detected acetylation on all of the subunits of
390 complex V that reside or extend into the mitochondrial matrix (ATP5A1, ATP5B, ATP5C1, ATP5D,
391 ATP5E, ATP5F1, ATP5H, ATP5J and ATP5O), while we only detect acetylation on two of the
392 membrane-embedded subunits (ATP5L and MT-ATP8), despite detecting a further four membrane-
393 embedded subunits in the proteome (ATP5I, ATP5J2, MT-ATP6 and USMG5). Indeed, the majority
394 of acetylated proteins quantified on each electron transport chain complex (CI-CV) are exposed to
395 either the mitochondrial matrix or the intermembrane space. Similarly, TCA cycle enzymes, which
396 are localized to the mitochondrial matrix, displayed high acetylation intensity and stoichiometry in
397 the basal state and HIIT augmented levels of acetylation at every stage of the cycle (Figure 6B), again

398 likely due to their proximity to acetyl-CoA. Conversely, cytosolic proteins regulating skeletal muscle
399 contraction showed fewer upregulated acetyl-sites with a number of downregulated sites following
400 HIIT (Figure 6C). Thus, proteins in close proximity to acetyl-CoA appear to be more susceptible to
401 acetylation.
402
403 Despite widespread HIIT-induced acetylation of mitochondrial proteins, these data should be
404 considered in the context of acetylation stoichiometry, which is generally low (Weinert et al., 2015).
405 Median acetylation stoichiometry in rodent liver has been calculated at only 0.05%, which increases
406 slightly to 0.11% for mitochondrial proteins (Weinert et al., 2015). Although acetylation is tissue-
407 dependent (Lundby et al., 2012), skeletal muscle levels are unlikely to be vastly different. The median
408 $\log_2$-fold change for mitochondrial acetyl-sites following HIIT was 0.9 (the corresponding value in
409 the proteome was 0.3), indicating that median post-HIIT stoichiometry would have remained at less
410 than 1%. Thus, the levels of HIIT-induced changes in acetylation may not be large enough to
411 influence gross activity on most metabolic enzymes. Nonetheless, physiological acetylation may be
412 high enough to be regulatory on some proteins. For example, acetylation of mitochondrial malate
413 dehydrogenase (MDH2) negatively correlates with its enzyme activity (Overmyer et al., 2015).
414 Another such enzyme could be pyruvate dehydrogenase (PDH), whose E1 component subunit alpha
415 (PDHA1) is within the top 25 most acetylated proteins (Supplementary File 6), whilst PDHA1 Lys
416 336 was within the top 5 most upregulated acetyl-sites with exercise training (Figure 5A). Increased
417 acetylation of PDHA1 occurs alongside suppressed enzyme activity in SIRT3 knockout mice (Jing et
418 al., 2013). By catalyzing the reaction between pyruvate and acetyl-CoA, PDH provides the link
419 between glycolysis and the tricarboxylic acid cycle (Constantin-Teodosiu, Constantin, Stephens,
420 Laithwaite, & Greenhaff, 2012). Thus, exercise-induced hyperacetylation of PDH could play a role
421 in the metabolic switch towards elevated fat oxidation following exercise training. Furthermore,

422 mitochondrial hyperacetylation increases fatty acid-supported respiration (Williams et al., 2020).
423 These data are consistent with the concomitant increase in acetylation (Figure 5A) and mitochondrial
424 respiratory capacity and fat oxidation (Figure 1F) following HIIT, suggesting that hyperacetylation
425 of mitochondrial proteins following exercise training may support the bioenergetic adaptations to
426 exercise.
427
428 **HIIT increases histone acetylation**
429 Aside from metabolic enzymes and contractile proteins, histones are regulated by acetylation (Sterner
430 & Berger, 2000; Strahl & Allis, 2000) and may represent a more specifically regulated pool of
431 proteins, owing to the nuclear localization of acetyltransferases (Hendzel, Sun, Chen, Rattner, &
432 Davie, 1994). Increases in certain acetylated histone residues are well characterized to augment
433 transcription, with exercise known to acutely regulate H3 acetylation (e.g. H3 K4, H3 K9/14 & H3
434 K36) (Joseph, Ayeleso, & Mukwevho, 2017; Lochmann, Thomas, Bennett, & Taylor, 2015; McGee,
435 Fairlie, Garnham, & Hargreaves, 2009; Smith, Kohn, Chetty, & Ojuka, 2008). Here we identified 18
436 distinct acetylated peptides from histones, with acetylated peptides from H1.5 (HIST1H1B K48),
437 H2B type 2F (HIST2H2BF K16/20) and H3.3 (H3F3B K23) being elevated following HIIT (Figs.
438 7A-D). H1.5 K48 was exclusively quantified in post-HIIT samples, however, it was only quantified
439 in 4 out of 7 of the post-HIIT samples, which is our minimum cut-off for valid values. The regulatory
440 roles of these HIIT-regulated histone acetyl-sites are unknown. However, acetylation of the N-
441 terminal of H2B, including K16 & K20, has been linked to transcriptional activation (H. Chen et al.,
442 2014; Parra, Kerr, Fahy, Pouchnik, & Wyrick, 2006), including the expression of NAD-metabolic
443 genes in yeast (Parra et al., 2006). The role of H3 K23 is also obscure, however, its acetylation
444 contributes to the development of cancer through the recruitment of the transcription factor
445 transcription intermediary factor 1-alpha (TRIM24) and the nuclear receptor estrogen receptor alpha

446 (ERS1) (Lv et al., 2017; Tsai et al., 2010), augmenting expression of phosphatidylinositol 4,5-
447 biphosphate 3-kinase catalytic subunit alpha (PIK3CA), a subunit of phosphoionositide-3-kinase
448 (PI3K), and phosphorylation of protein kinase B (AKT1) (Lv et al., 2017). Indeed, TRIM24 promotes
449 the abundance of glycolytic and TCA cycle genes in transforming human mammary epithelial cells
450 (Pathiraja et al., 2015), while ERS1 regulates mitochondrial biogenesis in skeletal muscle (Ribas et
451 al., 2016). Whether H3 K23 regulates TRIM24, ERS1, PI3K, and AKT1 activity and influences
452 metabolism in skeletal muscle remains unclear. Further studies are warranted to understand the
453 transcriptional and metabolic implications of exercise training-induced acetylation on these histone
454 sites.
455
456 Histone acetyltransferase p300 (EP300) is a nuclear-localized acetyltransferase targeting numerous
457 histone acetylation sites (Weinert et al., 2018). Therefore, we hypothesized that EP300 may be
458 involved in the regulation of histone acetylation following exercise training. Similarly to the
459 upregulation of acetylation on H2B K16/20 and H3 K23, HIIT increased the protein abundance of
460 EP300 by 23% (participant 1 was excluded as an outlier) (Figure 7E). Next, to investigate the
461 potential regulatory role of EP300 in the acetylation of these exercise-responsive histone sites in
462 skeletal muscle, we knocked down EP300 in C2C12 myotubes and assessed the acetylation of H2B
463 K20 and H3 K23 via immunoblotting. Knockdown of EP300 reduced acetylation of H2B K20 by
464 48%, whilst acetylation of H3 K23 was unaffected (Figure 7F). Together, these analyses identify
465 EP300 as an exercise-training responsive acetyltransferase, which regulates the acetylation of H2B
466 K20 in skeletal muscle.
467
468 **Conclusion**

469 Here, we leveraged advances in DIA mass spectrometry to produce a deep human skeletal muscle
470 proteome and applied this approach to ascertain exercise training adaptations. Furthermore, we
471 provide the first investigation of the human acetylome in response to exercise training. In the
472 proteome, we highlight known and novel exercise-responsive proteins, including a potential
473 mechanism to explain altered skeletal muscle calcium sensitivity following HIIT. In the acetylome,
474 we describe the predominant acetylation of mitochondrial proteins after HIIT, particularly of TCA
475 cycle proteins and subunits of electron transport chain complex V, as well as highlighting the
476 regulation of novel exercise-responsive histone acetyl-sites. Altogether, we provide a substantial
477 hypothesis-generating resource, identifying novel exercise-regulated proteins and acetyl-sites with
478 the aim of stimulating further mechanistic research investigating how exercise improves metabolic
479 health.
480

481 **Materials and Methods**

482 *Participants*

483 Participants were enrolled by AKL and MH between August and September 2017. Eight men were
484 assessed for eligibility. All eight men were eligible and gave their informed consent after receiving
485 written and oral information about the study and potential risks associated with the experimental
486 procedures (Figure 1-figure supplement 1). Inclusion criteria were healthy males, 18-40 years old,
487 $\dot{V}O_{2max}$ between 45-55 $mL \cdot min^{-1} \cdot kg^{-1}$ or 3000-4000 $mL \cdot min^{-1}$ and BMI between 19-26 $kg \cdot m^{-2}$.
488 Exclusion criteria were abnormal electrocardiogram, chronic disease, ongoing medical treatment, and
489 smoking. Subject characteristics are presented in Table 1. The study was approved by the National
490 Committee on Health Research Ethics (H-17004045) and registered at clinicaltrials.gov
491 (NCT03270475). The study complied with the Declaration of Helsinki (2013).

492

493 *Study outcomes*

494 The pre-determined primary outcome was the change from baseline in the skeletal muscle proteome.
495 Secondary outcomes were changes from baseline in the skeletal muscle acetylome, skeletal muscle
496 mitochondrial respiration and whole-body maximal oxygen consumption ($\dot{V}O_{2max}$).

497

498 *Experimental trials*

499 The study consisted of two experimental days separated by five weeks of high-intensity interval
500 training (HIIT). At each experimental day, body composition was measured by dual-energy X-ray
501 absorptiometry (DXA) scans (Lunar iDXA, GE Healthcare, GE Medical systems, Belgium). Then,
502 subjects rested in a supine position for 15 min and two 4 mm incisions separated by 2 cm were made
503 in the above the *vastus lateralis* muscle under local anaesthesia (Xylocaine 20 mg $mL^{-1}$ without
504 epinephrine, AstraZeneca, London, UK) and a muscle biopsy was taken from each incision using a
505 Bergström needle with suction. Afterwards, $\dot{V}O_{2max}$ was determined by indirect calorimetry using a
506 breath-by-breath gas analyser (Oxycon Pro, CareFusion, San Diego, USA) during an incremental test
507 on a bike ergometer (Monark LC4, Monark Exercise, Vansbro, Sweden). The incremental test
508 consisted of 5 min rest followed by 4 min stages at 50, 100, 150 W, after which the resistance was
509 increased in increments of 30 $W \cdot min^{-1}$ until exhaustion. Time to exhaustion was used to calculate
510 incremental peak power output (iPPO) accounting for time spent at the last increment. Subjects
511 completed the experimental protocol the same time of day before and after the intervention and were
512 instructed to eat a small meal with 500 mL water two hours before arriving at the laboratory. In
513 addition, subjects abstained from alcohol, caffeine, and physical activity for 48 h before each
514 experimental day and were instructed to maintain their activity level and diet during the study. The
515 experimental days were performed three days before and after the first and last training, respectively.

All experimental trials were performed at the Department of Nutrition, Exercise and Sports, University of Copenhagen. Experimental trials were completed in October 2017.

*Body composition*

At each experimental day, two scans were performed to reduce scan-to-scan variation (Nana, Slater, Hopkins, & Burke, 2012). Before the first scanning, subjects rested in a supine position for 10 min to allow fluid distribution reducing intra-scan variation (Berg, Tedner, & Tesch, 1993; Cerniglia, Delmonico, Lindle, Hurley, & Rogers, 2007). Whole-body and leg composition were calculated using software (enCORE Forma v. 15, GE Healthcare Lunar, Buckinghamshire, UK).

*Substrate utilization*

Gas exchange measurements during rest and submaximal exercise were used to calculate fat and glucose oxidative as previously described (Jeukendrup & Wallis, 2005) and corrected for protein oxidation (Lee, Day, Greenfield, & Ho, 2013). Fat oxidation and carbohydrate oxidation were calculated as:

$$Fat\ Oxidation\left(\frac{mg}{min}\right) = \left(1.695 \cdot \dot{V}O_2 - 1.701 \cdot \dot{V}CO_2\right) - \frac{1.92 \cdot 0.14 \cdot BM}{1440}$$

$$Carbohydrate\ Oxidation\left(\frac{mg}{min}\right) = \left(4.344 \cdot \dot{V}CO_2 - 3.061 \cdot \dot{V}O_2\right) - \frac{2.87 \cdot 0.14 \cdot BM}{1440}$$

where $\dot{V}O_2$ and $\dot{V}CO_2$ are in $L \cdot min^{-1}$ and *BM (Body mass)* is in kg.

*Muscle biopsies*

Immediately after collection, muscle biopsies were rinsed in ice-cold saline. A small piece (~15 mg) of the muscle was transferred into ice-cold preservation solution (BIOPS) for analysis of mitochondrial respiratory capacity. The remaining muscle tissue was snap-frozen in liquid nitrogen

539 and stored at –80°C. The frozen muscle samples were freeze-dried for 48 h and dissected free from
540 connective tissues, fat and blood under a microscope in a humidity-controlled room (~25% humidity)
541 before storage at –80°C for later analyses.
542
543 *High intensity interval training*
544 Subjects underwent a five-week high-intensity interval training intervention consisting of three
545 weekly training sessions with 4-5 × 4 min intervals interspersed by two min active recovery on indoor
546 spinning bikes. The training volume increased from four intervals during the first two weeks to five
547 intervals during the last three weeks. During each interval, subjects were instructed to reach >90% of
548 maximal heart rate ($HR_{max}$). All training sessions were supervised and subjects received verbal
549 encouragement during all intervals. The mean $HR_{max}$ during intervals was 96 ± 1% of $HR_{max}$.
550
551 *Mitochondrial profiling*
552 Mitochondrial respiratory capacity was determined in duplicate by high-resolution respirometry
553 (Oxygraph-2k, Oroboros Instruments, Innsbruck, Austria) at 37°C using 1-3 mg wet weight muscle
554 fibers per chamber in MiR06. Oxygen concentrations were kept between 200 and 450 µM throughout
555 the experiment. The muscle sample in BIOPS was prepared for high-resolution respirometry as
556 previously described (Pesta & Gnaiger, 2012). In short, muscle fibers were dissected free from
557 connective tissue and fat followed by permeabilization in BIOPS with saponin and washed in
558 mitochondrial respiration buffer (MiR06). A substrate-uncoupler-inhibitor titration protocol was used
559 to assess different respiratory states as previously described (Pesta et al., 2011). Leak respiration ($L_N$)
560 in the absence of adenylates was induced by the addition of malate (2 mM) and octanoylcarnitine (0.2
561 mM). Fatty acid oxidation (FAO) was determined after titration of ADP (2.5 mM). Submaximal CI
562 and CI+II-linked respiration ($CI_D$ & $P_D$) was measured in the presence of glutamate (10 mM) and

563 succinate (10 mM), respectively. Oxidative phosphorylation capacity (P) was assessed after another
564 titration of ADP (2.5 mM). The mitochondrial outer membrane integrity was then tested with the
565 addition of cytochrome C (10 µM). The average change in oxygen flux was 3.8% (range: 0.2-9.4%).
566 Respiratory electron transfer-pathway capacity (E) was measured during step-wise (0.5 µM) titration
567 of carbonyl cyanide p-trifluoro-methoxyphenyl hydrazine (FCCP). Succinate-supported electron
568 transfer-pathway capacity ($E_{CII}$) was assessed by the addition of rotenone (0.5 µM). Residual oxygen
569 consumption was determined after the addition of malonic acid (5 mM), myxothaizol (0.5 µM) and
570 antimycin A (2.5 µM) and subtracted from each respiratory state.
571
572 Maximal enzyme activity of citrate synthase was determined from muscle homogenate using
573 fluorometry (Fluoroscan Ascent, Thermo Fisher Scientific, Waltham, USA) at 25°C as previously
574 described (Lowry, 2012).
575
576 *Proteomic sample preparation*
577 Human skeletal muscles were lysed in a buffer consisting of 1% Sodium Deoxycholate (SDC), 10
578 mM Tris (2-carboxyethyl) phosphine (TCEP), 40 mM Chloroacetamide (CAA) and 100 mM of Tris
579 (pH 8.5). The muscles were homogenized with an Ultra Turrax homogenizer (IKA). Lysates were
580 boiled at 95°C for 10 min and sonicated using a tip sonicator. Lysates were then centrifuged at 16000g
581 for 10 min. Proteins were digested using the endoproteinases LysC and trypsin (1:100 w/w) at 37°C
582 overnight with shaking. Digested peptides were acidified using 1% Trifluoroacetic acid (TFA) and
583 precipitated SDC was removed by centrifugation. Peptides were purified using Sep-pak C18
584 cartridges (Waters) and were eluted in 50% acetonitrile. 20 µg of peptides were saved for total
585 proteome analysis while 3 mg peptides were saved for enrichment of acetylated peptides.
586

587 *Acetylated peptide enrichment*

588 The acetyl peptide enrichment was performed on 3 mg of digested peptides using PTMscan Acetyl-
589 Lysine Motif kit (Cell Signaling #13416). The peptides were mixed with 100 µL of 10x IP buffer
590 (500 mM MOPS, pH 7.2, 100 mM Na-phosphate, 500 mM NaCl, 5% NP-40). The acetonitrile was
591 removed and the volume was reduced to ~1mL by vacuum centrifugation. The final volume was
592 adjusted with water to a concentration of 3 $mg \cdot mL^{-1}$. The peptides were clarified by centrifugation at
593 20000g for 5 min. 20 µL of anti-acetylated lysine antibody was washed 3 times in 1 mL IP buffer and
594 then mixed with the peptides. Peptides were enriched overnight at 4°C, washed 3 times in 1 mL ice-
595 cold (4°C) IP buffer, 4 times in 1 mL ice-cold IP buffer without NP-40, and once in 1 mL water. All
596 wash buffer was removed via aspiration. Acetylated peptides were eluted with 100 µL 0.15% TFA.
597 The elution procedure was repeated three times. The eluted peptides were de-salted on C18 stage-tips
598 (Rappsilber, Mann, & Ishihama, 2007), vacuum concentrated and resuspended in buffer A* (5%
599 acetonitrile, 0.1% trifluoroacetic acid).

600

601 *High pH reversed-phase fractionation*

602 To generate a deep proteome library for data-independent acquisition (DIA), 50 µg of peptide was
603 pooled from pre- and post-HIIT samples, separately, and fractionated using high pH reversed-phase
604 chromatography (Kulak, Geyer, & Mann, 2017). 24 fractions (per pool) were automatically
605 concatenated using a rotor valve shift of 90 s. Approximately 0.3 µg of each fraction were subjected
606 to LC-MS/MS measurements via data-dependent acquisition (DDA). To obtain comprehensive
607 coverage of the acetylome, acetylated peptides from each sample were fractionated into 8 fractions
608 using a rotor valve shift of 90 s. For the first subject (both pre and post samples) all 8 fractions were
609 analysed separately. After observing lower than expected peptide intensities for the first subject, the

610 neighboring two factions were pooled together for each of the remaining samples (total four
611 fractions/subject/timepoint) before LC-MS analysis.
612
613 *Mass spectrometry*
614 Peptides were measured using LC-MS instrumentation consisting of an Easy nanoflow HPLC system
615 (Thermo Fisher Scientific, Bremen, Germany) coupled via a nanoelectrospray ion source (Thermo
616 Fischer Scientific, Bremen, Germany) to a Q Exactive HF-X mass spectrometer. Purified peptides
617 were separated on a 50 cm C18 column (inner diameter 75 µm, 1.8 µm beads, Dr. Maisch GmbH,
618 Germany). Peptides were loaded onto the column with buffer A (0.5% formic acid) and eluted with
619 a 100 min linear gradient increasing from 2-40% buffer B (80% acetonitrile, 0.5% formic acid). After
620 the gradient, the column was washed with 90% buffer B and re-equilibrated with buffer A. Peptides
621 were measured in singleton.
622
623 For the deep proteome library generation, mass spectra were acquired from each fraction via DDA
624 with automatic switching between MS and MS/MS using a top 15 method. MS spectra were acquired
625 in the Orbitrap analyzer with a mass range of 300-1750 m/z and 60,000 resolutions at m/z 200 with
626 a target of 3 x $10^6$ ions and a maximum injection time of 25 ms. HCD peptide fragments acquired at
627 27 normalized collision energy were analyzed at 15000 resolution in the Orbitrap analyzer with a
628 target of 1 x 105 ions and a maximum injection time of 28 ms. The mass spectra for the acetylome
629 experiments were also acquired from each fraction via DDA with a similar MS method used for deep
630 proteome library generation, except the maximum injection time for the fragment ion spectra was set
631 to 250 ms. A DIA MS method was used for the total proteome measurements in which one full scan
632 (300 to 1650 *m/z*, resolution = 60,000 at 200 *m/z*) at a target of 3 x $10^6$ ions was first performed,
633 followed by 32 windows with a resolution of 30000 where precursor ions were fragmented with

634 higher-energy collisional dissociation (stepped collision energy 25%, 27.5%, 30%) and analyzed with
635 an AGC target of 3 x $10^6$ ions and maximum injection time at 54 ms in profile mode using positive
636 polarity.
637
638 *Data processing*
639 Raw MS files from the experiments measured in DDA mode (muscle proteome library & acetylome),
640 were processed using MaxQuant (J. Cox & Mann, 2008). MS/MS spectra were searched by the
641 Andromeda search engine (integrated into MaxQuant) against the decoy UniProt-human database
642 (downloaded in December 2017) with forward and reverse sequences. In the main Andromeda search
643 precursor, mass and fragment mass were matched with an initial mass tolerance of 6 ppm and 20
644 ppm, respectively. The search included variable modifications of methionine oxidation and N-
645 terminal acetylation and fixed modification of carbamidomethyl cysteine. For the raw files from the
646 acetylome experiments, acetylated lysine was also added as a variable modification. Acetylated
647 peptides were filtered for a minimum Andromeda score of 40, as per the default settings for modified
648 peptides. The false discovery rate (FDR) was estimated for peptides and proteins individually using
649 a target-decoy approach allowing a maximum of 1% false identifications from a revered sequence
650 database. Raw files acquired in the DIA mode (total proteome) were processed using Biognosys
651 Spectronaut software version 13 (Bruderer et al., 2015). A single peptide library was generated in
652 Spectronaut using the combined MaxQuant search results for the DDA runs from both of the
653 fractionated muscle samples. The experimental DIA runs were then analyzed in Spectronaut using
654 default settings.
655
656 *Bioinformatics*

657 Bioinformatic analyses were performed in the Perseus software (Tyanova et al., 2016). Categorical
658 annotations were supplied in the form of Gene Ontology (GO) biological process (BP), molecular
659 function (MF), and cellular component (CC), as well as UniProt Keywords, KEGG and REACTOME
660 pathways. All annotations were extracted from the UniProt database. Quantified proteins were filtered
661 to have at least 4 valid values in at least one time point. Missing data were imputed by drawing
662 random numbers from a Gaussian distribution with a standard deviation of 30% and a downshift of
663 1.8 standard deviations from the mean. The imputed values have been tuned in order to simulate the
664 distribution of lowly abundant proteins. To identify differentially regulated proteins and acetyl-sites,
665 two-tailed paired *t*-tests were performed with a permutation-based false discovery correction applied
666 (FDR = 0.05). In the acetylome, an additional analysis was performed to expand the identification of
667 differentially expressed proteins, whereby an *a posteriori* information fusion scheme combining the
668 biological relevance (fold change) and the statistical significance (p-value), was implemented, as
669 previously described (Xiao et al., 2014). A Π-value significance score cut-off of 0.05 was selected.
670 Alterations to organelles were assessed using summed total protein abundances (Wisniewski, 2017)
671 and two-tailed paired t-tests ($p < 0.05$). Comparisons between individual proteins measured via
672 immunoblotting were performed using two-tailed paired t-tests ($p < 0.05$). Hierarchical clustering
673 analysis was performed on z-scored differentially regulated proteins using Euclidean distance.
674 Enrichment analyses were performed on differentially regulated proteins and acetyl-sites using
675 Fisher's exact tests and the application of a Benjamini-Hochberg false discovery correction (FDR =
676 0.02), as is the default setting in the Perseus software (Tyanova et al., 2016). Motif enrichment was
677 performed on upregulated acetyl-sites using iceLogo ($p < 0.01$) (Colaert et al., 2009). One-
678 dimensional enrichment analyses were performed as previously described (Juergen Cox & Mann,
679 2012). To analyze the relative stoichiometries of acetylated proteins in Figure 4 abundance corrected
680 intensities (ACIs) were calculated for each acetyl-peptide by dividing the acetyl-peptide intensity by

681 the intensity of the corresponding protein in the proteome. Enrichment analyses were performed
682 against a background of all quantified proteins or acetyl-sites, except for hierarchical clustering
683 analyses where clusters were compared within the z-scored differentially regulated matrix. To
684 visualize complexes and functional protein-interactions in Figure 6, protein interaction networks were
685 mapped using the STRING database, using an overall confidence cutoff of 0.7 without limiting the
686 number of interactions (Szklarczyk et al., 2019), and further processed with Cytoscape
687 (www.cytoscape.org).
688
689 *Cell culture*
690 The mouse skeletal muscle cell line C2C12 (CRL1772, ATCC) was seeded into six-well plates at a
691 density of $10^5$ cells per well. Cells were cultured in growth medium (Dulbeccoo's modified Eagle's
692 medium containing 25 mM glucose, supplemented with 10% fetal bovine serum (FBS) and 1%.
693 Penicillin-streptomycin) at 37°C and 5% $CO_2$. Once the cells reached ~90% confluency,
694 differentiation was induced by replacing the FBS with 2% horse serum. On day 4 of differentiation,
695 cells were transfected with 25mM EP300 siRNA or scramble control siRNA via the TransIT-X2
696 Dynamic Delivery System (Mirus Bio), following the manufacturer's instructions. Cells were
697 harvested in 2% SDS on Day 6. Samples were immediately boiled at 95°C, sonicated in a Diagenode
698 Bioruptor water bath sonicator (15 x 30s intervals), and centrifuged at 16000g for 10 min. The pellet
699 was discarded and the supernatant was taken and used for immunoblotting analyses.
700
701 *Immunoblotting*
702 For human skeletal muscle immunoblot analyses, a fresh batch of ice-cold homogenization buffer
703 (10% glycerol, 20 mM Na-pyrophosphate, 150 mM NaCl, 50 mM HEPES (pH 7.5), 1% NP-40, 20
704 mM β-glycerophosphate, 2 mM $Na_3VO_4$, 10 mM NaF, 2 mM PMSF, 1 mM EDTA (pH 8), 1 mM

705 EGTA (pH 8), 10 μg·mL$^{-1}$ Aprotinin, 10 μg·mL$^{-1}$ Leupeptin and 3 mM Benzamidine) was prepared
706 and 80 μL added to 1 mg of freeze-dried and dissected muscle tissue. The tissue was homogenized
707 for 1 min at 28.5 Hz in a TissueLyser (Qiagen TissueLyser II, Retsch GmbH, Germany) before
708 samples were rotated end over end for 1 hour at 4°C and centrifuged at 18320g for 20 min at 4°C.
709 The pellet was discarded and the supernatant was taken and used for immunoblotting analyses. Total
710 protein concentration in the samples was determined with a standard BSA kit (Millipore). 15 μL of
711 the sample was diluted with 60 μL ultrapure water in order to keep the concentration within the linear
712 range of the calibration curve (0.2 to 2 μg·μL$^{-1}$). The protein concentration of each sample was
713 adjusted by the addition of 6 × Laemmli buffer (7 mL 0.5M Tris-base, 3 mL glycerol, 0.93 g DTT, 1
714 g SDS and 1.2 mg bromophenol blue) and ultrapure water to reach equal concentrations (1.5 μg total
715 protein·μL$^{-1}$). Human skeletal muscle standard samples (Ctrl) were obtained as a pool of all samples
716 included in the experiment.
717
718 Equal amounts of total protein were loaded on 10% TGX Stain-Free, 4-20% TGX Stain-Free, or
719 16.5% Criterion Tris-Tricine/Peptide gels (Bio-Rad) alongside two protein markers (Precision plus
720 all blue and dual color standards, Bio-Rad), three human skeletal muscle control samples and a four-
721 point standard curve (skeletal muscle samples of increasing volume). After standard SDS-page gel
722 electrophoresis proteins were semi-dry transferred to a PVDF membrane. Membranes were blocked
723 with either 2% skimmed milk or 3% BSA in Tris-buffered saline with 0.1% Tween-20 (TBST) before
724 overnight incubation with primary antibody. Afterwards, the membranes were washed in TBST,
725 incubated for 1 hour in HRP conjugated secondary antibody at room temperature and washed 3 × 15
726 min in TBST before the bands were visualized with an enhanced chemiluminescent reaction
727 (Immobilon Forte Western HRP substrate, Millipore) and signals recorded with a digital camera
728 (ChemiDoc MP Imaging System, Bio-Rad). Densitometry quantification of the immunoblotting band

729 intensities was done using Image Lab version 4 (Bio-Rad) and determined as the total band intensity
730 adjusted for the background intensity. The standard curve on each gel was used to confirm that the
731 loaded amount of protein in samples was capable of determining differences between samples by the
732 signal intensity being on the linear part of the standard curve. The variation of the triplicate human
733 standard sample signal loaded was used to evaluate equal transfer of proteins across each gel.
734 Coomassie staining was conducted to confirm equal loading and transfer of total protein from the
735 different samples. Immunoblotting of biological samples was performed in singleton, with the
736 exception of EP300 which was performed in technical triplicates to confirm the presence of a
737 biological outlier (participant 1).
738
739 Listed are the primary antibodies used and, where appropriate, their size of migration. Acetyl-lysine:
740 #9441, Cell Signaling Technologies; EP300: #sc32244 (human skeletal muscle); #sc48343 (C2C12s),
741 Santa Cruz Biotechnology, 300 kDa; ac-H2B K20: #ab177430, Abcam, 14 kDa; H2B: #12364, Cell
742 Signaling Technologies, 14 kDa; ac-H3 K23: #14932, Cell Signaling Technologies, 17 kDa; H3:
743 #4499, Cell Signaling Technologies, 17 kDa; MYLK2: PA5-29324, Invitrogen, 65 kDa; OXPHOS
744 antibody cocktail: ab110411, Abcam, 15-55 kDa; SIRT1: 07-131, Millipore, 80 kDa; SIRT3: #5490,
745 Cell Signaling Technologies, 28 kDa; SIRT5: #8782, Cell Signaling Technologies, 30 kDa; SIRT6:
746 #12486, Cell Signaling Technologies, 36-42 kDa. The anti-GCN5L1 antibody (15 kDa) was a kind
747 gift from Iain Scott, PhD, University of Pittsburgh (Scott, Webster, Li, & Sack, 2012; Thapa et al.,
748 2020). HRP conjugated goat anti-rabbit (4010-05, SouthernBiotech) and a goat anti-mouse (P0447,
749 DAKO Denmark) were used as secondary antibodies.
750
751 *Statistical analyses*

752 For non-omics analyses, two-tailed paired t-tests were applied to assess the effect of HIIT, except for
753 substrate oxidation analyses whereby a mixed linear model was performed. Independent samples two-
754 tailed t-tests were used to assess the effect of EP300 KD on histone acetylation. Significance was
755 accepted as $p < 0.05$.
756

757 **Acknowledgements**

758 This work was supported by an unconditional donation from the Novo Nordisk Foundation (NNF) to
759 NNF Center for Basic Metabolic Research (http://www.cbmr.ku.dk) (Grant number
760 NNF18CC0034900), NNF Center for Protein Research (https://www.cpr.ku.dk/) (Grant number
761 NNF14CC001), and Team Denmark. We would like to acknowledge Matthias Mann, Jens Jung
762 Nielsen, Rebeca Soria Romero and the mass spectrometry platform from at the NNF Center for
763 Protein Research for technical assistance and access to mass spectrometers. We would like to thank
764 Iain Scott from the University of Pittsburgh Department of Medicine for the kind gift of the anti-
765 GCN5L1 antibody.

766

767 **Competing interests**

768 The authors declare no competing interests.

769

770 **Materials & Correspondence**

771 Requests for reagents and resources should be directed to Atul S. Deshmukh (atul.deshmukh@sund.ku.dk).

## Supplementary Tables

***Supplementary File 1.*** *Identified proteins.*

***Supplementary File 2.*** *Quantified proteins and their regulation by HIIT.*

***Supplementary File 3.*** *Fisher's exact test of HIIT-regulated proteins (FDR < 0.05).*

***Supplementary File 4.*** *Identified acetyl-sites.*

***Supplementary File 5.*** *Quantified acetyl-sites and their regulation by HIIT.*

***Supplementary File 6.*** *Summed acetylation intensity per protein.*

***Supplementary File 7.*** *One-dimensional enrichment analysis of summed acetylation intensity.*

***Supplementary File 8.*** ***A****bundance corrected intensities (ACIs) of acetyl-sites pre-HIIT.*

***Supplementary File 9.*** *One-dimensional enrichment analysis of pre-HIIT acetyl-site ACI (Leading protein ID was used for relative enrichment).*

***Supplementary File 10.*** *Fisher's exact test of HIIT-regulated (ΠI < 0.05) acetyl-sites (Leading protein ID was used for relative enrichment).*

https://drive.google.com/drive/folders/13Hx0NcA66gY6Fl-5L3NjFov0F4KoH36H?usp=sharing

797 **Figure Legends**

798 ***Figure 1.*** **Physiological adaptations to HIIT**

799 **A**. Experimental overview. **B**. Subject characteristics. **C**. Five weeks of HIIT increased maximal
800 oxygen uptake ($\dot{V}O_{2max}$) and incremental peak power output (iPPO). **D** HIIT increased whole-body
801 fat oxidation during submaximal exercise (50-150 W) without altering **E**. carbohydrate oxidation. **F**.
802 HIIT increased mitochondrial respiration in skeletal muscle ($L_N$: leak respiration, FAO: fatty acid
803 oxidation, $CI_D$: submaximal CI respiration, $P_D$: submaximal CI+II respiration, P: oxidative
804 phosphorylation capacity, E: electron transport system capacity, $E_{CII}$: succinate-supported electron
805 transport system capacity). **G**. HIIT increased skeletal muscle citrate synthase (CS) activity. **H**.
806 Analytical workflow. Summary statistics are mean ± SEM (n = 8). * $p < 0.05$, ** $p < 0.01$, *** $p <$
807 $0.001$.

808

809 ***Figure 2.*** **HIIT increases mitochondrial proteins and reduces a subset of contractile fiber**
810 **associated proteins**

811 **A**. Volcano plot displaying 102 upregulated and 24 downregulated proteins following HIIT (FDR <
812 0.05). **B**. Fisher's exact tests identified the enrichment of mitochondrial terms within the differentially
813 regulated proteins (enrichment analysis FDR < 0.02). **C**. Hierarchical clustering and enrichment
814 analysis (enrichment analysis FDR < 0.02) on differentially regulated proteins identified that
815 mitochondrial terms are enriched within the upregulated proteins, while cytoplasm (UniProt
816 Keyword) is enriched amongst the downregulated proteins. **D**. Summed total protein abundances for
817 different organelles (UniProt Keyword) shows upregulation of the mitochondrial protein content. **E-**
818 **G**. Summed total protein abundances display upregulation of electron transport chain complexes (**E**.),
819 mitochondrially-encoded proteins (**F**.) and proteins with a transit peptide (**G**.). Summary statistics are
820 mean ± SEM (n = 8). * $p < 0.05$, ** $p < 0.01$, *** $p < 0.001$.

821

822 ***Figure 3.*** **HIIT regulates proteins involved in skeletal muscle calcium sensitivity and handling**

823 HIIT did not alter the abundance of myosin heavy chain (MYH1: MyHC2x, MYH2: MyHC2a,
824 MYH4: MyHC2x, MYH7: MyHCβ; **A**.) or light chain (**B**.) isoforms. **C**. HIIT regulates proteins
825 controlling myosin phosphorylation. **D**. HIIT reduces abundance of subunits of the dihydropyridine
826 receptor. **E**. Summed total protein abundances display downregulation of the dihydropyridine
827 receptor. **F**. HIIT does not alter the abundance of ryanodine receptor 1. Summary statistics are mean
828 ± SEM (n = 8). ^ FDR < 0.05. * p < 0.05, ** p < 0.01, *** p < 0.001.

829

830 ***Figure 4.*** **The human skeletal muscle acetylome displays higher stoichiometry on mitochondrial**
831 **proteins and lower stoichiometry on contractile proteins**

832 **A**. We quantified 1263 acetyl-sites corresponding to 464 proteins (n = 7). Of these, 421 proteins were
833 also quantified in the proteome with 1232 of the quantified acetyl-sites located on these 421 proteins.
834 **B**. Distribution of acetyl-sites on proteins within the pre-HIIT acetylome. **C**. Top 10 highest intensity
835 acetylated proteins (acetyl-peptide intensities were summed for each protein) within the pre-HIIT
836 acetylome. **D**. Cumulative protein abundance and rank within the proteome (the top 10 highest
837 intensity acetyl-proteins are highlighted). **E**. One-dimensional enrichment analysis of acetylated
838 protein intensity identified mitochondrial proteins, particularly those involved in carboxylic acid
839 metabolism and monovalent inorganic cation transport (e.g. complex V) as having systematically
840 high acetylation intensities (enrichment analysis FDR < 0.02). **F**. Top 10 acetyl-sites with highest
841 abundance-corrected intensities (ACIs). **G**. One-dimensional enrichment analysis of acetyl-site ACIs
842 identified mitochondrial and carboxylic acid catabolic proteins as higher stoichiometry (positive
843 enrichment factor), while contractile fiber cytosolic and plasma membrane proteins were enriched
844 as lower stoichiometry (negative enrichment factor; (enrichment analysis FDR < 0.02; enrichment

845 performed on leading protein IDs). **H**. Histogram depicting the ACI distribution of the total acetylome
846 (blue), the mitochondrial acetyl-sites (green) and the contractile fiber acetyl-sites (yellow).
847 Mitochondrial proteins were distributed at higher ACI values and contractile fiber proteins at lower
848 ACI values than the total acetylome.
849
850 ***Figure 5*. HIIT increases acetylation of mitochondrial and TCA cycle proteins concomitantly**
851 **with an increase in SIRT3 abundance**
852 **A**. Volcano plot displaying 20 upregulated (filled red circles) and 1 downregulated (filled blue circle)
853 acetyl-sites following HIIT at an FDR < 0.05, while 257 acetyl-sites were upregulated (red circles)
854 and 26 downregulated (blue circles) at Π < 0.05 (n = 7). **B**. Scatter plot indicating that HIIT-induced
855 changes in acetyl-site intensity typically exceeded that of the corresponding protein. **C**. Fisher's exact
856 tests identified the enrichment of mitochondrial and TCA cycle terms within the differentially
857 regulated acetyl-proteins (enrichment analysis FDR < 0.02; enrichment performed on leading protein
858 IDs). **D**. IceLogo motif enrichment (p < 0.01) for the upregulated sites displayed a predominance of
859 proximal cysteine residues relative to the acetylated lysine (position 0). **E**. Immunoblotting analysis
860 identified the upregulation of the deacetylases SIRT3, SIRT5, and SIRT6, but no change in SIRT1,
861 whilst the mitochondrial acetyltransferase GCN5L1 remained unchanged following HIIT (n = 7-8).
862 Representative images confirming equal loading are displayed in Figure 5-figure supplement 2. * p
863 < 0.05, ** p < 0.01, *** p < 0.001.
864
865 ***Figure 6*. Individual acetyl-site regulation of mitochondrial, TCA cycle and contractile proteins**
866 **following HIIT**

867 Regulation of acetyl-sites on **A**. electron transport chain complex subunits (annotated by HUGO), **B**.
868 TCA cycle proteins (annotated by KEGG) and **C**. muscle contraction proteins (annotated by
869 REACTOME).
870
871 ***Figure 7*. HIIT increases acetylation on specific histone acetyl-sites**
872 HIIT increased acetylation on **A**. H1.5 K48, **B**. H2B type 2F K16/20 and **C**. H3 K23. **D**. HIIT did not
873 alter H4 acetylation (n = 7). **E.** Immunoblotting analysis identified the upregulation of the nuclear-
874 localized acetyltransferase EP300 (n = 8, mean of three technical replicates; participant 1 was
875 excluded as an outlier from statistical analysis (pre, post and fold-change values were all >3 median
876 absolute deviations from the respective median), data for participant 1 is shown in the translucent
877 data points). **F.** Knockdown of EP300 reduces acetylation of H2B K20 but not H3 K23 in C2C12
878 myotubes (n = 3). Representative images confirming equal loading are displayed in Figure 5-figure
879 supplement 2. Summary statistics are mean ± SEM. † $\Pi < 0.05$. * $p < 0.05$, ** $p < 0.01$, *** $p <$
880 $0.001$.
881
882 ***Figure 1-figure supplement 1.* CONSORT flow diagram of enrolled participants**
883
884 ***Figure 1-figure supplement 2.* Proteome quality control**
885 **A**. Quantified proteins from each sample. **B**. Representative Pearson correlation between biological
886 replicates (Pre 4 v Pre 5). **C**. Cellular compartment (GOCC) coverage of the proteome. **D**. Principal
887 component analysis of the proteome. P: participant.
888
889 ***Figure 2-figure supplement 1*. HIIT increases electron transport chain subunits**

890 Immunoblotting analyses confirmed the upregulation of electron transport chain proteins.
891 Representative images confirming equal loading are displayed in Figure 5-figure supplement 2.
892 Summary statistics are mean ± SEM (n = 8). * $p < 0.05$, ** $p < 0.01$, *** $p < 0.001$.
893
894 ***Figure 3-figure supplement 1***. **HIIT decreases MYLK2 abundance**
895 **A**. Immunoblotting analysis confirms the downregulation of MYLK2. Representative images
896 confirming equal loading are displayed in Figure 5-figure supplement 2. **B**. No change in the
897 abundance of sarcoplasmic/endoplasmic reticulum calcium ATPases 1-3 (SERCAs). Summary
898 statistics are mean ± SEM (n = 8). * $p < 0.05$, ** $p < 0.01$, *** $p < 0.001$.
899
900 ***Figure 4-figure supplement 1.*** **Acetylome quality control**
901 **A**. Overlap between identified acetyl-site with those identified in human skeletal muscle by Lundby
902 et al. (2012). **B**. Quantified acetyl-sites from each sample. **C**. Representative Pearson correlation
903 between biological replicates (Pre 4 v Pre 5). **D**. Cellular compartment (GOCC) coverage of the
904 acetylome. **E**. Principal component analysis of the acetylome. P: participant.
905
906 ***Figure 5-figure supplement 1.*****HIIT increases protein acetylation**
907 Immunoblotting analysis confirmed the upregulation of acetylation following HIIT (n = 7).
908 Representative images confirming equal loading are displayed in Figure 5-figure supplement 2. * p
909 $< 0.05$, ** $p < 0.01$, *** $p < 0.001$.
910
911 ***Figure 5-figure supplement 2.*** **Representative images of equal loading for immunoblot analyses**
912 **A**. Coomassie stain for n = 8 immunoblots of human skeletal muscle (Figure 5E (SIRT1-6), Figure
913 7E, Figure 2-figure supplement 1, and Figure 3-figure supplement 1). **B**. Stain-free image for n = 7

914 immunoblots of human skeletal muscle (Figure 5E (GCN5L1), and Figure 5-figure supplement 1).

915 **C**. Stain-free image for EP300 KD immunoblots (Figure 7F).

916

## References


Alessi, D., MacDougall, L. K., Sola, M. M., Ikebe, M., & Cohen, P. (1992). The control of protein phosphatase-1 by targetting subunits. The major myosin phosphatase in avian smooth muscle is a novel form of protein phosphatase-1. *European Journal of Biochemistry, 210*(3), 1023-1035. doi:10.1111/j.1432-1033.1992.tb17508.x

Baeza, J., Smallegan, M. J., & Denu, J. M. (2016). Mechanisms and Dynamics of Protein Acetylation in Mitochondria. *Trends in Biochemical Sciences, 41*(3), 231-244. doi:10.1016/j.tibs.2015.12.006

Banas, K., Clow, C., Jasmin, B. J., & Renaud, J. M. (2011). The KATP channel Kir6.2 subunit content is higher in glycolytic than oxidative skeletal muscle fibers. *American Journal of Physiology: Regulatory, Integrative and Comparative Physiology, 301*(4), R916-925. doi:10.1152/ajpregu.00663.2010

Berg, H. E., Tedner, B., & Tesch, P. A. (1993). Changes in lower limb muscle cross-sectional area and tissue fluid volume after transition from standing to supine. *Acta Physiologica Scandinavica, 148*(4), 379-385. doi:10.1111/j.1748-1716.1993.tb09573.x

Braschi, B., Denny, P., Gray, K., Jones, T., Seal, R., Tweedie, S., . . . Bruford, E. (2019). Genenames.org: the HGNC and VGNC resources in 2019. *Nucleic Acids Research, 47*(D1), D786-D792. doi:10.1093/nar/gky930

Bruderer, R., Bernhardt, O. M., Gandhi, T., Miladinović, S. M., Cheng, L. Y., Messner, S., . . . Reiter, L. (2015). Extending the limits of quantitative proteome profiling with data-independent acquisition and application to acetaminophen-treated three-dimensional liver microtissues. *Molecular & Cellular Proteomics, 14*(5), 1400-1410. doi:10.1074/mcp.M114.044305

Campanella, M., Casswell, E., Chong, S., Farah, Z., Wieckowski, M. R., Abramov, A. Y., . . . Duchen, M. R. (2008). Regulation of Mitochondrial Structure and Function by the F1Fo-ATPase Inhibitor Protein, IF1. *Cell Metabolism, 8*(1), 13-25. doi:10.1016/j.cmet.2008.06.001

Cerniglia, L. M., Delmonico, M. J., Lindle, R., Hurley, B. F., & Rogers, M. A. (2007). Effects of acute supine rest on mid-thigh cross-sectional area as measured by computed tomography. *Clinical Physiology and Functional Imaging, 27*(4), 249-253. doi:10.1111/j.1475-097X.2007.00742.x

Chen, H., Ruiz, P. D., Novikov, L., Casill, A. D., Park, J. W., & Gamble, M. J. (2014). MacroH2A1.1 and PARP-1 cooperate to regulate transcription by promoting CBP-mediated H2B acetylation. *Nature Structural & Molecular Biology, 21*(11), 981-989. doi:10.1038/nsmb.2903

Chen, Y., Deng, Y., Zhang, J., Yang, L., Xie, X., & Xu, T. (2009). GDI-1 preferably interacts with Rab10 in insulin-stimulated GLUT4 translocation. *Biochemical Journal, 422*(2), 229-235. doi:10.1042/bj20090624

Choudhary, C., Weinert, B. T., Nishida, Y., Verdin, E., & Mann, M. (2014). The growing landscape of lysine acetylation links metabolism and cell signalling. *Nature Reviews Molecular Cell Biology, 15*(8), 536-550. doi:10.1038/nrm3841

Christensen, P. M., Jacobs, R. A., Bonne, T., Flück, D., Bangsbo, J., & Lundby, C. (2016). A short period of high-intensity interval training improves skeletal muscle mitochondrial function and pulmonary oxygen uptake kinetics. *J Appl Physiol (1985), 120*(11), 1319-1327. doi:10.1152/japplphysiol.00115.2015

Cohen, P. (2000). The regulation of protein function by multisite phosphorylation--a 25 year update. *Trends in Biochemical Sciences, 25*(12), 596-601. doi:10.1016/s0968-0004(00)01712-6

Colaert, N., Helsens, K., Martens, L., Vandekerckhove, J., & Gevaert, K. (2009). Improved visualization of protein consensus sequences by iceLogo. *Nat Methods, 6*(11), 786-787. doi:10.1038/nmeth1109-786

Constantin-Teodosiu, D., Carlin, J. I., Cederblad, G., Harrist, R. C., & Hultman, E. (1991). Acetyl group accumulation and pyruvate dehydrogenase activity in human muscle during incremental exercise. *Acta Physiologica Scandinavica, 143*(4), 367-372. doi:10.1111/j.1748-1716.1991.tb09247.x

Constantin-Teodosiu, D., Constantin, D., Stephens, F., Laithwaite, D., & Greenhaff, P. L. (2012). The role of FOXO and PPAR transcription factors in diet-mediated inhibition of PDC activation and carbohydrate oxidation during exercise in humans and the role of pharmacological activation of PDC in overriding these changes. *Diabetes, 61*(5), 1017-1024. doi:10.2337/db11-0799

Cox, J., & Mann, M. (2008). MaxQuant enables high peptide identification rates, individualized p.p.b.-range mass accuracies and proteome-wide protein quantification. *Nature Biotechnology, 26*(12), 1367-1372. doi:10.1038/nbt.1511

Cox, J., & Mann, M. (2012). 1D and 2D annotation enrichment: a statistical method integrating quantitative proteomics with complementary high-throughput data. *BMC Bioinformatics, 13 Suppl 16*(Suppl 16), S12-S12. doi:10.1186/1471-2105-13-S16-S12

Davis, J. S., Hassanzadeh, S., Winitsky, S., Lin, H., Satorius, C., Vemuri, R., . . . Epstein, N. D. (2001). The overall pattern of cardiac contraction depends on a spatial gradient of myosin regulatory light chain phosphorylation. *Cell, 107*(5), 631-641. doi:10.1016/s0092-8674(01)00586-4

Deshmukh, A. S., Murgia, M., Nagaraj, N., Treebak, J. T., Cox, J., & Mann, M. (2015). Deep proteomics of mouse skeletal muscle enables quantitation of protein isoforms, metabolic pathways, and transcription factors. *Molecular & Cellular Proteomics, 14*(4), 841-853. doi:10.1074/mcp.M114.044222

Deshmukh, A. S., Steenberg, D. E., Hostrup, M., Birk, J. B., Larsen, J. K., Santos, A., . . . Wojtaszewski, J. F. P. (2021). Deep muscle-proteomic analysis of freeze-dried human muscle biopsies reveals fiber type-specific adaptations to exercise training. *Nature Communications, 12*(1), 304. doi:10.1038/s41467-020-20556-8

Deutscher, M. P. (1984). The eucaryotic aminoacyl-tRNA synthetase complex: suggestions for its structure and function. *The Journal of Cell Biology, 99*(2), 373-377. doi:10.1083/jcb.99.2.373

Dohlmann, T. L., Hindsø, M., Dela, F., Helge, J. W., & Larsen, S. (2018). High-intensity interval training changes mitochondrial respiratory capacity differently in adipose tissue and skeletal muscle. *Physiological Reports, 6*(18), e13857. doi:10.14814/phy2.13857

Du, J., Zhou, Y., Su, X., Yu, J. J., Khan, S., Jiang, H., . . . Lin, H. (2011). Sirt5 is a NAD-dependent protein lysine demalonylase and desucciinylase. *Science, 334*(6057), 806-809. doi:10.1126/science.1207861

Egan, B., & Zierath, J. R. (2013). Exercise metabolism and the molecular regulation of skeletal muscle adaptation. *Cell Metabolism, 17*(2), 162-184. doi:10.1016/j.cmet.2012.12.012

Flucher, B. E., & Franzini-Armstrong, C. (1996). Formation of junctions involved in excitation-contraction coupling in skeletal and cardiac muscle. *Proceedings of the National Academy of Sciences of the United States of America, 93*(15), 8101-8106. doi:10.1073/pnas.93.15.8101

Foster, D. B., Liu, T., Rucker, J., O'Meally, R. N., Devine, L. R., Cole, R. N., & O'Rourke, B. (2013). The Cardiac Acetyl-Lysine Proteome. *PloS One, 8*(7), e67513. doi:10.1371/journal.pone.0067513

Freeman, H. C., Hugill, A., Dear, N. T., Ashcroft, F. M., & Cox, R. D. (2006). Deletion of Nicotinamide Nucleotide Transhydrogenase. *Diabetes, 55*(7), 2153. doi:10.2337/db06-0358

Gibala, M. J., MacLean, D. A., Graham, T. E., & Saltin, B. (1998). Tricarboxylic acid cycle intermediate pool size and estimated cycle flux in human muscle during exercise. *American Journal of Physiology, 275*(2), E235-242. doi:10.1152/ajpendo.1998.275.2.E235

Gonzalez-Franquesa, A., Stocks, B., Chubanava, S., Hattel, H. B., Moreno-Justicia, R., Peijs, L., . . . Deshmukh, A. S. (2021). Mass-spectrometry-based proteomics reveals mitochondrial supercomplexome plasticity. *Cell Rep, 35*(8), 109180. doi:10.1016/j.celrep.2021.109180

Granata, C., Oliveira, R. S., Little, J. P., Renner, K., & Bishop, D. J. (2016). Training intensity modulates changes in PGC-1alpha and p53 protein content and mitochondrial respiration, but not markers of mitochondrial content in human skeletal muscle. *FASEB Journal, 30*(2), 959-970. doi:10.1096/fj.15-276907

Hansen, B. K., Gupta, R., Baldus, L., Lyon, D., Narita, T., Lammers, M., . . . Weinert, B. T. (2019). Analysis of human acetylation stoichiometry defines mechanistic constraints on protein regulation. *Nature Communications, 10*(1), 1055. doi:10.1038/s41467-019-09024-0

Hebert, A. S., Dittenhafer-Reed, K. E., Yu, W., Bailey, D. J., Selen, E. S., Boersma, M. D., . . . Coon, J. J. (2013). Calorie restriction and SIRT3 trigger global reprogramming of the mitochondrial protein acetylome. *Molecular Cell, 49*(1), 186-199. doi:10.1016/j.molcel.2012.10.024

Hendzel, M. J., Sun, J. M., Chen, H. Y., Rattner, J. B., & Davie, J. R. (1994). Histone acetyltransferase is associated with the nuclear matrix. *Journal of Biological Chemistry, 269*(36), 22894-22901.

Hirschey, M. D., Shimazu, T., Goetzman, E., Jing, E., Schwer, B., Lombard, D. B., . . . Verdin, E. (2010). SIRT3 regulates mitochondrial fatty-acid oxidation by reversible enzyme deacetylation. *Nature, 464*(7285), 121-125. doi:10.1038/nature08778

Ho, H.-Y., Lin, Y.-T., Lin, G., Wu, P.-R., & Cheng, M.-L. (2017). Nicotinamide nucleotide transhydrogenase (NNT) deficiency dysregulates mitochondrial retrograde signaling and impedes proliferation. *Redox Biology, 12*, 916-928. doi:https://doi.org/10.1016/j.redox.2017.04.035

Hoek, J. B., & Rydström, J. (1988). Physiological roles of nicotinamide nucleotide transhydrogenase. *Biochemical Journal, 254*(1), 1-10. doi:10.1042/bj2540001

Hoffman, N. J., Parker, B. L., Chaudhuri, R., Fisher-Wellman, K. H., Kleinert, M., Humphrey, S. J., . . . James, D. E. (2015). Global phosphoproteomic analysis of human skeletal muscle reveals a network of exercise-regulated kinases and AMPK substrates. *Cell Metabolism, 22*(5), 922-935. doi:10.1016/j.cmet.2015.09.001

Holloway, K. V., O'Gorman, M., Woods, P., Morton, J. P., Evans, L., Cable, N. T., . . . Burniston, J. G. (2009). Proteomic investigation of changes in human vastus lateralis muscle in response to interval-exercise training. *Proteomics, 9*(22), 5155-5174. doi:10.1002/pmic.200900068

Hostrup, M., & Bangsbo, J. (2017). Limitations in intense exercise performance of athletes – effect of speed endurance training on ion handling and fatigue development. *The Journal of Physiology, 595*(9), 2897-2913. doi:10.1113/JP273218

Hostrup, M., Gunnarsson, T. P., Fiorenza, M., Mørch, K., Onslev, J., Pedersen, K. M., & Bangsbo, J. (2019). In-season adaptations to intense intermittent training and sprint interval training in sub-elite football players. *Scandinavian Journal of Medicine and Science in Sports, 29*(5), 669-677. doi:10.1111/sms.13395

Hostrup, M., Onslev, J., Jacobson, G. A., Wilson, R., & Bangsbo, J. (2018). Chronic β(2) -adrenoceptor agonist treatment alters muscle proteome and functional adaptations induced by high intensity training in young men. *Journal of Physiology, 596*(2), 231-252. doi:10.1113/jp274970

Howlett, R. A., Parolin, M. L., Dyck, D. J., Hultman, E., Jones, N. L., Heigenhauser, G. J., & Spriet, L. L. (1998). Regulation of skeletal muscle glycogen phosphorylase and PDH at varying exercise power outputs. *American Journal of Physiology, 275*(2 Pt 2), R418-425.

Jacobs, R. A., Flück, D., Bonne, T. C., Bürgi, S., Christensen, P. M., Toigo, M., & Lundby, C. (2013). Improvements in exercise performance with high-intensity interval training coincide with an

increase in skeletal muscle mitochondrial content and function. *Journal of Applied Physiology, 115*(6), 785-793. doi:10.1152/japplphysiol.00445.2013

James, A. M., Smith, A. C., Smith, C. L., Robinson, A. J., & Murphy, M. P. (2018). Proximal Cysteines that Enhance Lysine N-Acetylation of Cytosolic Proteins in Mice Are Less Conserved in Longer-Living Species. *Cell Rep, 24*(6), 1445-1455. doi:10.1016/j.celrep.2018.07.007

Jeukendrup, A. E., & Wallis, G. A. (2005). Measurement of substrate oxidation during exercise by means of gas exchange measurements. *International Journal of Sports Medicine, 26 Suppl 1*, S28-37. doi:10.1055/s-2004-830512

Jing, E., O'Neill, B. T., Rardin, M. J., Kleinridders, A., Ilkeyeva, O. R., Ussar, S., . . . Kahn, C. R. (2013). Sirt3 regulates metabolic flexibility of skeletal muscle through reversible enzymatic deacetylation. *Diabetes, 62*(10), 3404-3417. doi:10.2337/db12-1650

Joseph, J. S., Ayeleso, A. O., & Mukwevho, E. (2017). Exercise increases hyper-acetylation of histones on the Cis-element of NRF-1 binding to the Mef2a promoter: Implications on type 2 diabetes. *Biochemical and Biophysical Research Communications, 486*(1), 83-87. doi:https://doi.org/10.1016/j.bbrc.2017.03.002

Kulak, N. A., Geyer, P. E., & Mann, M. (2017). Loss-less Nano-fractionator for High Sensitivity, High Coverage Proteomics. *Molecular & Cellular Proteomics, 16*(4), 694-705. doi:10.1074/mcp.O116.065136

Larsen, S., Danielsen, J. H., Søndergård, S. D., Søgaard, D., Vigelsoe, A., Dybboe, R., . . . Helge, J. W. (2015). The effect of high-intensity training on mitochondrial fat oxidation in skeletal muscle and subcutaneous adipose tissue. *Scandinavian Journal of Medicine and Science in Sports, 25*(1), e59-e69. doi:10.1111/sms.12252

Larsen, S., Nielsen, J., Hansen, C. N., Nielsen, L. B., Wibrand, F., Stride, N., . . . Hey-Mogensen, M. (2012). Biomarkers of mitochondrial content in skeletal muscle of healthy young human subjects. *The Journal of Physiology, 590*(14), 3349-3360. doi:10.1113/jphysiol.2012.230185

Lee, P., Day, R. O., Greenfield, J. R., & Ho, K. K. (2013). Formoterol, a highly β2-selective agonist, increases energy expenditure and fat utilisation in men. *International Journal of Obesity (2005), 37*(4), 593-597. doi:10.1038/ijo.2012.90

Lochmann, T. L., Thomas, R. R., Bennett, J. P., Jr., & Taylor, S. M. (2015). Epigenetic Modifications of the PGC-1α Promoter during Exercise Induced Expression in Mice. *PloS One, 10*(6), e0129647. doi:10.1371/journal.pone.0129647

Lowry, O. (2012). *A flexible system of enzymatic analysis*: Elsevier.

Ludwig, C., Gillet, L., Rosenberger, G., Amon, S., Collins, B. C., & Aebersold, R. (2018). Data-independent acquisition-based SWATH-MS for quantitative proteomics: a tutorial. *Molecular Systems Biology, 14*(8), e8126. doi:10.15252/msb.20178126

Lundby, A., Lage, K., Weinert, B. T., Bekker-Jensen, D. B., Secher, A., Skovgaard, T., . . . Olsen, J. V. (2012). Proteomic analysis of lysine acetylation sites in rat tissues reveals organ specificity and subcellular patterns. *Cell Rep, 2*(2), 419-431. doi:10.1016/j.celrep.2012.07.006

Lv, D., Jia, F., Hou, Y., Sang, Y., Alvarez, A. A., Zhang, W., . . . Feng, H. (2017). Histone Acetyltransferase KAT6A Upregulates PI3K/AKT Signaling through TRIM24 Binding. *Cancer Research, 77*(22), 6190-6201. doi:10.1158/0008-5472.Can-17-1388

Lynch, G. S., McKenna, M. J., & Williams, D. A. (1994). Sprint-training effects on some contractile properties of single skinned human muscle fibres. *Acta Physiologica Scandinavica, 152*(3), 295-306. doi:10.1111/j.1748-1716.1994.tb09809.x

Majerczak, J., Karasinski, J., & Zoladz, J. A. (2008). Training induced decrease in oxygen cost of cycling is accompanied by down-regulation of SERCA expression in human vastus lateralis muscle. *Journal of Physiology and Pharmacology, 59*(3), 589-602.

Mandsager, K., Harb, S., Cremer, P., Phelan, D., Nissen, S. E., & Jaber, W. (2018). Association of Cardiorespiratory Fitness With Long-term Mortality Among Adults Undergoing Exercise Treadmill Testing. *JAMA Network Open, 1*(6), e183605-e183605. doi:10.1001/jamanetworkopen.2018.3605

McGee, S. L., Fairlie, E., Garnham, A. P., & Hargreaves, M. (2009). Exercise-induced histone modifications in human skeletal muscle. *Journal of Physiology, 587*(Pt 24), 5951-5958. doi:10.1113/jphysiol.2009.181065

Meinild Lundby, A. K., Jacobs, R. A., Gehrig, S., de Leur, J., Hauser, M., Bonne, T. C., . . . Lundby, C. (2018). Exercise training increases skeletal muscle mitochondrial volume density by enlargement of existing mitochondria and not de novo biogenesis. *Acta Physiol (Oxf), 222*(1), e12905-n/a. doi:10.1111/apha.12905

Munkvik, M., Rehn, T. A., Slettaløkken, G., Hasic, A., Hallén, J., Sjaastad, I., . . . Lunde, P. K. (2010). Training effects on skeletal muscle calcium handling in human chronic heart failure. *Medicine and Science in Sports and Exercise, 42*(5), 847-855. doi:10.1249/MSS.0b013e3181c29ec1

Murgia, M., Toniolo, L., Nagaraj, N., Ciciliot, S., Vindigni, V., Schiaffino, S., . . . Mann, M. (2017). Single Muscle Fiber Proteomics Reveals Fiber-Type-Specific Features of Human Muscle Aging. *Cell Rep, 19*(11), 2396-2409. doi:10.1016/j.celrep.2017.05.054

Nana, A., Slater, G. J., Hopkins, W. G., & Burke, L. M. (2012). Effects of Daily Activities on Dual-Energy X-ray Absorptiometry Measurements of Body Composition in Active People. *Medicine and Science in Sports and Exercise, 44*(1), 180-189. doi:10.1249/MSS.0b013e318228b60e

Narita, T., Weinert, B. T., & Choudhary, C. (2019). Functions and mechanisms of non-histone protein acetylation. *Nature Reviews: Molecular Cell Biology, 20*(3), 156-174. doi:10.1038/s41580-018-0081-3

Ortenblad, N., Lunde, P. K., Levin, K., Andersen, J. L., & Pedersen, P. K. (2000). Enhanced sarcoplasmic reticulum Ca(2+) release following intermittent sprint training. *American Journal of Physiology: Regulatory, Integrative and Comparative Physiology, 279*(1), R152-160. doi:10.1152/ajpregu.2000.279.1.R152

Overmyer, K. A., Evans, C. R., Qi, N. R., Minogue, C. E., Carson, J. J., Chermside-Scabbo, C. J., . . . Burant, C. F. (2015). Maximal oxidative capacity during exercise is associated with skeletal muscle fuel selection and dynamic changes in mitochondrial protein acetylation. *Cell Metabolism, 21*(3), 468-478. doi:10.1016/j.cmet.2015.02.007

Parker, B. L., Kiens, B., Wojtaszewski, J. F. P., Richter, E. A., & James, D. E. (2020). Quantification of exercise-regulated ubiquitin signaling in human skeletal muscle identifies protein modification cross talk via NEDDylation. *FASEB Journal, 34*(4), 5906-5916. doi:https://doi.org/10.1096/fj.202000075R

Parra, M. A., Kerr, D., Fahy, D., Pouchnik, D. J., & Wyrick, J. J. (2006). Deciphering the roles of the histone H2B N-terminal domain in genome-wide transcription. *Molecular and Cellular Biology, 26*(10), 3842-3852. doi:10.1128/MCB.26.10.3842-3852.2006

Pathiraja, T. N., Thakkar, K. N., Jiang, S., Stratton, S., Liu, Z., Gagea, M., . . . Barton, M. C. (2015). TRIM24 links glucose metabolism with transformation of human mammary epithelial cells. *Oncogene, 34*(22), 2836-2845. doi:10.1038/onc.2014.220

Peng, C., Lu, Z., Xie, Z., Chen, Y., Tan, M., Luo, H., . . . Zhao, Y. (2011). The first identification of lysine malonylation substrates and its regulatory enzyme. *Molecular & Cellular Proteomics, 10*(12), M111.012658. doi: 10.1074/mcp/M111.012658

Pesta, D., & Gnaiger, E. (2012). High-resolution respirometry: OXPHOS protocols for human cells and permeabilized fibers from small biopsies of human muscle. *Methods in Molecular Biology, 810*, 25-58. doi:10.1007/978-1-61779-382-0_3

Pesta, D., Hoppel, F., Macek, C., Messner, H., Faulhaber, M., Kobel, C., . . . Gnaiger, E. (2011). Similar qualitative and quantitative changes of mitochondrial respiration following strength and endurance training in normoxia and hypoxia in sedentary humans. *American Journal of Physiology: Regulatory, Integrative and Comparative Physiology, 301*(4), R1078-R1087. doi:10.1152/ajpregu.00285.2011

Pietrocola, F., Galluzzi, L., Bravo-San Pedro, José M., Madeo, F., & Kroemer, G. (2015). Acetyl Coenzyme A: A Central Metabolite and Second Messenger. *Cell Metabolism, 21*(6), 805-821. doi:https://doi.org/10.1016/j.cmet.2015.05.014

Pougovkina, O., te Brinke, H., Ofman, R., van Cruchten, A. G., Kulik, W., Wanders, R. J., . . . de Boer, V. C. (2014). Mitochondrial protein acetylation is driven by acetyl-CoA from fatty acid oxidation. *Human Molecular Genetics, 23*(13), 3513-3522. doi:10.1093/hmg/ddu059

Putman, C. T., Jones, N. L., Hultman, E., Hollidge-Horvat, M. G., Bonen, A., McConachie, D. R., & Heigenhauser, G. J. F. (1998). Effects of short-term submaximal training in humans on muscle metabolism in exercise. *American Journal of Physiology-Endocrinology and Metabolism, 275*(1), E132-E139. doi:10.1152/ajpendo.1998.275.1.E132

Rappsilber, J., Mann, M., & Ishihama, Y. (2007). Protocol for micro-purification, enrichment, pre-fractionation and storage of peptides for proteomics using StageTips. *Nature Protocols, 2*(8), 1896-1906. doi:10.1038/nprot.2007.261

Ribas, V., Drew, B. G., Zhou, Z., Phun, J., Kalajian, N. Y., Soleymani, T., . . . Hevener, A. L. (2016). Skeletal muscle action of estrogen receptor α is critical for the maintenance of mitochondrial function and metabolic homeostasis in females. *Science Translational Medicine, 8*(334), 334ra354. doi:10.1126/scitranslmed.aad3815

Robinson, M. M., Dasari, S., Konopka, A. R., Johnson, M. L., Manjunatha, S., Esponda, R. R., . . . Nair, K. S. (2017). Enhanced protein translation underlies improved metabolic and physical adaptations to different exercise training modes in young and old humans. *Cell Metabolism, 25*(3), 581-592. doi:10.1016/j.cmet.2017.02.009

Scott, I., Webster, B. R., Li, J. H., & Sack, M. N. (2012). Identification of a molecular component of the mitochondrial acetyltransferase programme: a novel role for GCN5L1. *The Biochemical Journal, 443*(3), 655-661. doi:10.1042/BJ20120118

Smith, J. A., Kohn, T. A., Chetty, A. K., & Ojuka, E. O. (2008). CaMK activation during exercise is required for histone hyperacetylation and MEF2A binding at the MEF2 site on the Glut4 gene. *American Journal of Physiology-Endocrinology and Metabolism, 295*(3), E698-704. doi:10.1152/ajpendo.00747.2007

St Clair, D. K., Wan, X. S., Oberley, T. D., Muse, K. E., & St Clair, W. H. (1992). Suppression of radiation-induced neoplastic transformation by overexpression of mitochondrial superoxide dismutase. *Molecular Carcinogenesis, 6*(4), 238-242. doi:10.1002/mc.2940060404

Sterner, D. E., & Berger, S. L. (2000). Acetylation of histones and transcription-related factors. *Microbiology and molecular biology reviews : MMBR, 64*(2), 435-459. doi:10.1128/mmbr.64.2.435-459.2000

Strahl, B. D., & Allis, C. D. (2000). The language of covalent histone modifications. *Nature, 403*(6765), 41-45. doi:10.1038/47412

Svinkina, T., Gu, H., Silva, J. C., Mertins, P., Qiao, J., Fereshetian, S., . . . Carr, S. A. (2015). Deep, Quantitative Coverage of the Lysine Acetylome Using Novel Anti-acetyl-lysine Antibodies and an Optimized Proteomic Workflow. *Molecular & Cellular Proteomics, 14*(9), 2429-2440. doi:10.1074/mcp.O114.047555

Szklarczyk, D., Gable, A. L., Lyon, D., Junge, A., Wyder, S., Huerta-Cepas, J., . . . Mering, C. V. (2019). STRING v11: protein-protein association networks with increased coverage,

supporting functional discovery in genome-wide experimental datasets. *Nucleic Acids Research, 47*(D1), D607-d613. doi:10.1093/nar/gky1131

Tabb, D. L., Vega-Montoto, L., Rudnick, P. A., Variyath, A. M., Ham, A.-J. L., Bunk, D. M., . . . Spiegelman, C. (2010). Repeatability and reproducibility in proteomic identifications by liquid chromatography-tandem mass spectrometry. *Journal of Proteome Research, 9*(2), 761-776. doi:10.1021/pr9006365

Tao, R., Coleman, M. C., Pennington, J. D., Ozden, O., Park, S. H., Jiang, H., . . . Gius, D. (2010). Sirt3-mediated deacetylation of evolutionarily conserved lysine 122 regulates MnSOD activity in response to stress. *Molecular Cell, 40*(6), 893-904. doi:10.1016/j.molcel.2010.12.013

Tao, Z., Gao, P., & Liu, H. W. (2009). Identification of the ADP-ribosylation sites in the PARP-1 automodification domain: Analysis and implications. *Journal of the American Chemical Society, 131*(40), 14258-14260. doi:10.1021/ja906135d

Thapa, D., Manning, J. R., Stoner, M. W., Zhang, M., Xie, B., & Scott, I. (2020). Cardiomyocyte-specific deletion of GCN5L1 in mice restricts mitochondrial protein hyperacetylation in response to a high fat diet. *Scientific Reports, 10*(1), 10665. doi:10.1038/s41598-020-67812-x

Tsai, W.-W., Wang, Z., Yiu, T. T., Akdemir, K. C., Xia, W., Winter, S., . . . Barton, M. C. (2010). TRIM24 links a non-canonical histone signature to breast cancer. *Nature, 468*(7326), 927-932. doi:10.1038/nature09542

Tyanova, S., Temu, T., Sinitcyn, P., Carlson, A., Hein, M. Y., Geiger, T., . . . Cox, J. (2016). The Perseus computational platform for comprehensive analysis of (prote)omics data. *Nature Methods, 13*, 731. doi:10.1038/nmeth.3901

Ubaida-Mohien, C., Gonzalez-Freire, M., Lyashkov, A., Moaddel, R., Chia, C. W., Simonsick, E. M., . . . Ferrucci, L. (2019). Physical Activity Associated Proteomics of Skeletal Muscle: Being Physically Active in Daily Life May Protect Skeletal Muscle From Aging. *Elife, 10*(312). doi:10.3389/fphys.2019.00312

Vassilopoulos, A., Pennington, J. D., Andresson, T., Rees, D. M., Bosley, A. D., Fearnley, I. M., . . . Gius, D. (2014). SIRT3 deacetylates ATP synthase F1 complex proteins in response to nutrient- and exercise-induced stress. *Antioxidants & redox signaling, 21*(4), 551-564. doi:10.1089/ars.2013.5420

Weinert, B. T., Iesmantavicius, V., Moustafa, T., Schölz, C., Wagner, S. A., Magnes, C., . . . Choudhary, C. (2014). Acetylation dynamics and stoichiometry in Saccharomyces cerevisiae. *Molecular Systems Biology, 10*(1), 716. doi:10.1002/msb.134766

Weinert, B. T., Moustafa, T., Iesmantavicius, V., Zechner, R., & Choudhary, C. (2015). Analysis of acetylation stoichiometry suggests that SIRT3 repairs nonenzymatic acetylation lesions. *EMBO Journal, 34*(21), 2620-2632. doi:10.15252/embj.201591271

Weinert, B. T., Narita, T., Satpathy, S., Srinivasan, B., Hansen, B. K., Schölz, C., . . . Choudary, C. (2018). Time-resolved analysis reveals rapid dynamics and broad scopeof the CBP/p300 acetylome. *Cell, 174*(1), 231-244. doi: 10.1016/j.cell.2018.04.033

Wen, D., Utesch, T., Wu, J., Robertson, S., Liu, J., Hu, G., & Chen, H. (2019). Effects of different protocols of high intensity interval training for VO2max improvements in adults: A meta-analysis of randomised controlled trials. *Journal of Science and Medicine in Sport, 22*(8), 941-947. doi:https://doi.org/10.1016/j.jsams.2019.01.013

Williams, A. S., Koves, T. R., Davidson, M. T., Crown, S. B., Fisher-Wellman, K. H., Torres, M. J., . . . Muoio, D. M. (2020). Disruption of acetyl-lysine turnover in muscle mitochondria promotes insulin resistance and redox stress without overt respiratory dysfunction. *Cell Metabolism, 31*(1), 131-147.e111. doi:https://doi.org/10.1016/j.cmet.2019.11.003

Wisniewski, J. R. (2017). Label-Free and Standard-Free Absolute Quantitative Proteomics Using the "Total Protein" and "Proteomic Ruler" Approaches. *Methods in Enzymology, 585*, 49-60. doi:10.1016/bs.mie.2016.10.002

Wooldridge, A. A., Fortner, C. N., Lontay, B., Akimoto, T., Neppl, R. L., Facemire, C., . . . Haystead, T. A. J. (2008). Deletion of the protein kinase A/protein kinase G target SMTNL1 promotes an exercise-adapted phenotype in vascular smooth muscle. *The Journal of Biological Chemistry, 283*(17), 11850-11859. doi:10.1074/jbc.M708628200

Xiao, Y., Hsiao, T. H., Suresh, U., Chen, H. I., Wu, X., Wolf, S. E., & Chen, Y. (2014). A novel significance score for gene selection and ranking. *Bioinformatics, 30*(6), 801-807. doi:10.1093/bioinformatics/btr671

1263 **Appendix 1 – Key Resource Table**

| Reagent type or resource | Designation | Source or reference | Identifiers | Additional information |
|---|---|---|---|---|
| Antibody | MYLK2 Antibody (rabbit polyclonal; 1:1000) | Invitrogen | Cat#PA5-29324<br>RRID: AB_2546800 | |
| Antibody | Total OXPHOS Human WB Antibody Cocktail (mouse monoclonal; 1:1000) | Abcam | Cat#ab110411<br>RRID: AB_2756818 | |
| Antibody | Sirt1(Sir2) Antibody (rabbit polyclonal; 1:1000) | Millipore Sigma | Cat#07-131<br>RRID: AB_10067921 | |
| Antibody | Sirt3 (D22A3) Antibody (rabbit monoclonal; 1:2000) | Cell Signaling Technologies | Cat#5490<br>RRID: AB_10828246 | |
| Antibody | Sirt5 Antibody (rabbit monoclonal; 1:1000) | Cell Signaling Technologies | Cat#8782<br>RRID: AB_2716763 | |
| Antibody | Sirt6 Antibody (rabbit monoclonal; 1:1000) | Cell Signaling Technologies | Cat#12486<br>RRID: AB_2636969 | |
| Antibody | Acetyl-lysine Antibody (rabbit polyclonal; 1:1000) | Cell Signaling Technologies | Cat#9441<br>RRID: AB_331805 | |
| Antibody | P300 Mouse Antibody (mouse monoclonal; 1:200) | Santa Cruz Biotechnologies | Cat#sc48343<br>RRID: AB_628075 | |
| Antibody | P300 Mouse Antibody (mouse monoclonal; 1:500) | Santa Cruz Biotechnologies | Cat#sc32244<br>RRID: AB_628076 | |

| | | | | |
|---|---|---|---|---|
| Antibody | Ac-H2B K20 Antibody (rabbit monoclonal; 1:1000) | Abcam | Cat#ab177430 | |
| Antibody | H2B Antibody (rabbit monoclonal; 1:3000) | Cell Signaling Technologies | Cat#12364<br>RRID: AB_2714167 | |
| Antibody | Ac-H3 K23 Antibody (rabbit monoclonal; 1:1000) | Cell Signaling Technologies | Cat#14932<br>RRID: AB_2798650 | |
| Antibody | H3 Antibody (rabbit monoclonal; 1:3000) | Cell Signaling Technologies | Cat#4499<br>RRID: AB_10544537 | |
| Antibody | Goat Anti-Rabbit Ig, Human ads-HRP (goat polyclonal; 1:5000) | Southern Biotech | Cat#4010-05<br>RRID: AB_2632593 | |
| Antibody | Goat Anti-Mouse (goat polyclonal; 1:5000) | Dako (Agilent) | Cat# P0447<br>RRID: AB_2617137 | |
| Biological sample (human) | Human skeletal muscle (*vastus lateralis)* | This paper | | |
| Cell line (mouse) | C2C12 (ATCC® CRL-1772™) | ATCC | Cat#1722<br>RRID: CVCL_0188 | Authenticated by ATCC – CO1 assay. Tested in-house for mycoplasma – negative. |
| Chemical compound, drug | Glycerol | Millipore Sigma | Cat# G5516; CAS# 56-81-5 | |

| | | | | |
|---|---|---|---|---|
| Chemical compound, drug | Sodium pyrophosphate decahydrate | Millipore Sigma | Cat# 221368; CAS# 13472-36-1 | |
| Chemical compound, drug | Sodium chloride | Millipore Sigma | Cat# S9888; CAS# 7647-14-5 | |
| Chemical compound, drug | HEPES | Millipore Sigma | Cat# H3375; CAS# 7365-45-9 | |
| Chemical compound, drug | IGEPAL CA-630, NP-40 | Millipore Sigma | Cat# I8896; CAS# 9002-93-1 | |
| Chemical compound, drug | β-Glycerophosphate disodium salt hydrate | Millipore Sigma | Cat# G9422; CAS# 154804-51-0 | |
| Chemical compound, drug | Sodium orthovanadate | Millipore Sigma | Cat# S6508; CAS# 13721-39-6 | |
| Chemical compound, drug | Sodium fluoride | Millipore Sigma | Cat# S1504; CAS# 7681-49-4 | |
| Chemical compound, drug | Phenylmethanesulfonyl fluoride | Millipore Sigma | Cat# P7626; CAS# 329-98-6 | |
| Chemical compound, drug | EDTA (for electrophoresis) | Millipore Sigma | Cat# E5134; CAS# 6381-92-6 | |

| | | | | |
|---|---|---|---|---|
| Chemical compound, drug | EGTA | Millipore Sigma | Cat# E4378; CAS# 67-42-5 | |
| Chemical compound, drug | Aprotinin from bovine lung | Millipore Sigma | Cat# A1153; CAS# 9087-70-1 | |
| Chemical compound, drug | Leupeptin | Millipore Sigma | Cat# L2884; CAS# 103476-89-7 | |
| Chemical compound, drug | Benzamidine hydrochloride hydrate | Millipore Sigma | Cat# B6506; CAS# 206752-36-5 | |
| Chemical compound, drug | Bovine serum albumin | Millipore Sigma | Cat# A7906; CAS# 9048-46-8 | |
| Chemical compound, drug | Trizma base | Millipore Sigma | Cat# T1503; CAS# 77-86-1 | |
| Chemical compound, drug | DL-Dithiothreitol | Millipore Sigma | Cat# D0632 and 43819; CAS# 3483-12-3 | |
| Chemical compound, drug | Sodium dodecyl sulfate | Millipore Sigma | Cat# L3771; CAS# 151-21-3 | |
| Chemical compound, drug | Bromophenol Blue sodium salt | Millipore Sigma | Cat# B8026; CAS# 34725-61-6 | |

| | | | | |
|---|---|---|---|---|
| Chemical compound, drug | Tween 20 | Millipore Sigma | Cat# P9416; CAS# 9005-64-5 | |
| Chemical compound, drug | Skimmed milk powder | Easis | Cat# 801300 | |
| Chemical compound, drug | Glycine | Millipore Sigma | Cat# G7126; CAS# 56-40-6 | |
| Chemical compound, drug | 2-propanol | Millipore Sigma | Cat# 109634; CAS# 67-63-0 | |
| Chemical compound, drug | Ethanol 96% | Plum | Cat# 201146; CAS# 64-17-5 | |
| Chemical compound, drug | Brilliant Blue R | Millipore Sigma | Cat# B7920; CAS# 6104-59-2 | |
| Chemical compound, drug | Acetic acid (glacial) 100% | Millipore Sigma | Cat# 100063; CAS# 64-19-7 | |
| Chemical compound, drug | Precision plus all blue | BioRad | Cat# 1610373 | |
| Chemical compound, drug | Precision plus dual color | BioRad | Cat# 1610374 | |

| | | | | |
|---|---|---|---|---|
| Chemical compound, drug | Immobilon Forte Western HRP substrate | Millipore Sigma | Cat# WBLUF 0500 | |
| Chemical compound, drug | Bovine Serum Albumin Standard | Thermo Fisher Scientific | Cat# 23209 | |
| Chemical compound, drug | BCA Protein Assay Reagent A | Thermo Fisher Scientific | Cat# 23223 | |
| Chemical compound, drug | BCA Protein Assay Reagent B | Thermo Fisher Scientific | Cat# 23224 | |
| Chemical compound, drug | Potassium phosphate dibasic trihydrate | Millipore Sigma | Cat# P9666; CAS# 16788-57-1 | |
| Chemical compound, drug | Potassium dihydrogen phosphate | Millipore Sigma | Cat# 1.04873; CAS# 7778-77-0 | |
| Chemical compound, drug | BCA Protein Assay Kit | Thermo Fisher Scientific | Cat# 23225 | |
| Chemical compound, drug | Trizma hydrochloride | Millipore Sigma | Cat# T3253; CAS# 1185-53-1 | |
| Chemical compound, drug | EDTA | Millipore Sigma | Cat# E9884; CAS# 60-00-4 | |

| | | | | |
|---|---|---|---|---|
| Chemical compound, drug | NAD | Millipore Sigma | Cat# NAD100-RO; CAS# 53-84-9 | |
| Chemical compound, drug | L-(−)-Malic acid sodium salt | Millipore Sigma | Cat# M1125; CAS# 68303-40-2 | |
| Chemical compound, drug | Acetyl-Coenzyme A | Millipore Sigma | Cat# ACOA-RO | |
| Chemical compound, drug | L-Malate Dehydrogenase (L-MDH) | Millipore Sigma | Cat# LMDH-RO | |
| Chemical compound, drug | NADH | Millipore Sigma | Cat# 10107735001 | |
| Chemical compound, drug | Sucrose | Millipore Sigma | Cat# S7903; CAS# 57-50-1 | |
| Chemical compound, drug | Magnesium chloride hexahydrate | Millipore Sigma | Cat# M2670; CAS# 7791-18-6 | |
| Chemical compound, drug | Taurine | Millipore Sigma | Cat# T0625; CAS# 107-35-7 | |
| Chemical compound, drug | Potassium Dihydrogen Phosphate | Millipore Sigma | Cat# P9791; CAS# 7778-77-0 | |

| | | | | |
|---|---|---|---|---|
| Chemical compound, drug | HEPES | Millipore Sigma | Cat# H3375; CAS# 7365-45-9 | |
| Chemical compound, drug | Bovine serum albumin (fatty acid free) | Millipore Sigma | Cat# A7030; CAS# 9048-46-8 | |
| Chemical compound, drug | Catalase from bovine liver | Millipore Sigma | Cat# C9322; CAS# 9001-05-2 | |
| Chemical compound, drug | Lactobionic acid | Millipore Sigma | Cat# 153516; CAS# 96-82-2 | |
| Chemical compound, drug | MES potassium salt | Millipore Sigma | Cat# M0895; CAS# 39946-25-3 | |
| Chemical compound, drug | ATP | Millipore Sigma | Cat# A3377; CAS# 34369-07-8 | |
| Chemical compound, drug | Sodium creatine phosphate dibasic tetrahydrate | Millipore Sigma | Cat# 27920; CAS# 71519-72-7 | |
| Chemical compound, drug | Imidazole | Millipore Sigma | Cat# I0250; CAS# 288-32-4 | |
| Chemical compound, drug | Potassium hydroxide | Millipore Sigma | Cat# P1767; CAS# 1310-58-3 | |

| | | | | |
|---|---|---|---|---|
| Chemical compound, drug | Calcium carbonate | Millipore Sigma | Cat# C4830; CAS# 471-34-1 | |
| Chemical compound, drug | Saponin from quillaja bark | Millipore Sigma | Cat# S7900; CAS# 8047-15-2 | |
| Chemical compound, drug | L-(−)-Malic acid sodium salt | Millipore Sigma | Cat# M1125; CAS# 68303-40-2 | |
| Chemical compound, drug | Octanoyl-L-carnitine | Millipore Sigma | Cat# 50892; CAS# 25243-95-2 | |
| Chemical compound, drug | ADP | Millipore Sigma | Cat# A5285; CAS# 72696-48-1 | |
| Chemical compound, drug | L-glutamic acid monosodium salt monohydrate | Millipore Sigma | Cat# 49621; CAS# 6106-04-3 | |
| Chemical compound, drug | Sodium succinate dibasic hexahydrate | Millipore Sigma | Cat# S2378; CAS# 6106-21-4 | |
| Chemical compound, drug | Cytochrome c from equine heart | Millipore Sigma | Cat# C2506; CAS# 9007-43-6 | |
| Chemical compound, drug | FCCP | Millipore Sigma | Cat# C2920; CAS# 370-86-5 | |

| | | | | |
|---|---|---|---|---|
| Chemical compound, drug | Rotenone | Millipore Sigma | Cat# R8875; CAS# 83-79-4 | |
| Chemical compound, drug | Malonic acid | Millipore Sigma | Cat# M1296; CAS# 141-82-2 | |
| Chemical compound, drug | Myxothiazol | Millipore Sigma | Cat# T5580; CAS# 76706-55-3 | |
| Chemical compound, drug | Antimycin A from Streptomyces sp. | Millipore Sigma | Cat# A8674; CAS# 1397-94-0 | |
| Chemical compound, drug | Sodium deoxycholate | Sigma-Aldrich | Cat# D6750<br>CAS# 302-95-4 | |
| Chemical compound, drug | Tris(2-carboxyethyl)phosphine hydrochloride | Sigma-Aldrich | Cat# C4706<br>CAS# 51805-45-9 | |
| Chemical compound, drug | 2-Chloroacetamide | Sigma-Aldrich | Cat# 22790<br>CAS# 79-07-2 | |
| Chemical compound, drug | Trypsin | Sigma-Aldrich | Cat# T7575 | |
| Chemical compound, drug | Lysine | Wako | Cat# 124-06871 | |

| | | | | |
|---|---|---|---|---|
| Chemical compound, drug | DMEM high glucose | Gibco | Cat# 41965039 | |
| Chemical compound, drug | Fetal bovine serum(FBS) | Sigma-Aldrich | Cat# F7524 | |
| Chemical compound, drug | Penicillin-Streptomycin, liquid | Gibco | Cat# 15070-063 | |
| Chemical compound, drug | Opti-MEM™ I Reduced Serum Medium | Gibco | Cat# 31985062 | |
| Chemical compound, drug | TransIT-X2 Dynamic Delivery System | Mirus Bio | Cat# MIR6003 | |
| Sequence-based reagent | EP300 siRNA | Merck Sigma | Cat# SASI_Mm01_00159721 | |
| Commercial assay or kit | PTMScan® Acetyl-Lysine Motif [Ac-K] Kit | Cell Signaling Technologies | Cat#13416 | |
| Software, algorithm, | Graphpad Prism 8.0 | https://www.graphpad.com/ | RRID: SCR_002798 | |
| Software, algorithm | MaxQuant 1.5.3.30 | https://maxquant.org/ | RRID: SCR_014485 | |
| Software, algorithm | Spectronaut v14 | https://biognosys.com/shop/spectronaut | | |

| | | | | |
|---|---|---|---|---|
| Software, algorithm | Perseus 1.6.10.50 | http://www.coxdocs.org/doku.php?id=perseus:start | RRID: SCR_015753 | |
| Software, algorithm | R Studio | https://rstudio.com/ | RRID: SCR_000432 | |
| Software, algorithm | Cytoscape v3.7.2 | www.cytoscape.org | RRID: SCR_003032 | |
| Software, algorithm | iceLogo | https://iomics.ugent.be/icelogoserver/ | RRID: SCR_012137 | |
| Software, algorithm | Adobe Illustrator 24.3 | https://www.adobe.com/products/illustrator | RRID: SCR_010279 | |
| Software, algorithm | Bio-Rad Image Studio | https://www.licor.com/bio/products/Software,algorithm/image_studio/ | RRID: SCR_014210 | |
| Software, algorithm | Oroboros DatLab 6 V. 6.1.0.7 | https://www.oroboros.at/index.php/product/datlab/ | | |
| Other | 10% Criterion TGX Stain-Free gel | BioRad | Cat# 567-8035 | |
| Other | 16.5% Criterion Tris-Tricine/Peptide gel | BioRad | Cat# 345-0065 | |
| Other | Immobilon-P PVDF membrane | Millipore Sigma | Cat# IPVH00010 | |

| | | | | |
|---|---|---|---|---|
| Other | Whatman cellulose chromatography papers | Millipore Sigma | Cat# WHA3030917 | |
| Other | Stainless Steel Beads 5mm | Qiagen | Cat# 69989 | |
| Other | Stuart Rotator Drive STR4 | Stuart-equipment | Cat# STR4 | |
| Other | Hettich universal 320 R centrifuge | Andrea Hettich GmbH, Germany | Cat# 1406 | |
| Other | $E_{max}$ precision microplate reader | Molecular Devices | Cat# LR88026 | |
| Other | PowerPac HC Power Supply | BioRad | Cat# 1645052 | |
| Other | TE 77 ECL Semi-Dry Transfer Unit | Amersham Biosciences | Cat# 80-6211-86 | |
| Other | ChemiDoc MP Imaging System | BioRad | Cat# 731BR00119 | |
| Other | White 96-Well Immuno Plates | Fischer Scientific | Cat# 10415985 | |
| Other | Fluoroskan, Microplate Fluorometer, one dispenser | Fischer Scientific | Cat# 5200111 | |
| Other | Non-treated 96-Well Microplates | Fischer Scientific | Cat# 10252711 | |
| Other | Multiskan FC Microplate Photometer | Fischer Scientific | Cat# 11500695 | |
| Other | Sep-Pak C18 Cartrige | Waters | Cat# WAT054955 | |

1264

1265

Figure 1

A

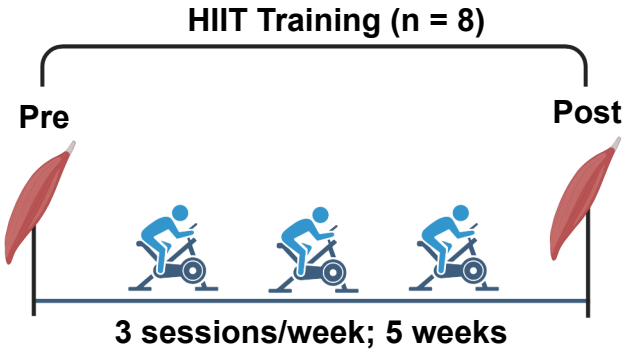


B

**Subject characteristics**

| | Pre | Post |
|---|---|---|
| Age (years) | 27 ± 2 | |
| Height (cm) | 187 ± 2 | |
| Weight (kg) | 82.2 ± 3.7 | 81.8 ± 3.4 |
| BMI (kg·m$^{-2}$) | 23.5 ± 0.9 | 23.4 ± 0.8 |
| Lean mass (kg) | 59.1 ± 1.2 | 60.1 ± 1.2** |
| Fat mass (kg) | 19.7 ± 2.9 | 18.9 ± 2.6 |
| $\dot{V}O_2$max (mL·min$^{-1}$) | 3669 ± 334 | 4200 ± 117*** |
| $\dot{V}O_2$max (mL·kg$^{-1}$·min$^{-1}$) | 45.3 ± 6.9 | 51.8 ± 1.9*** |
| iPPO (W) | 340 ± 18 | 400 ± 13*** |

C

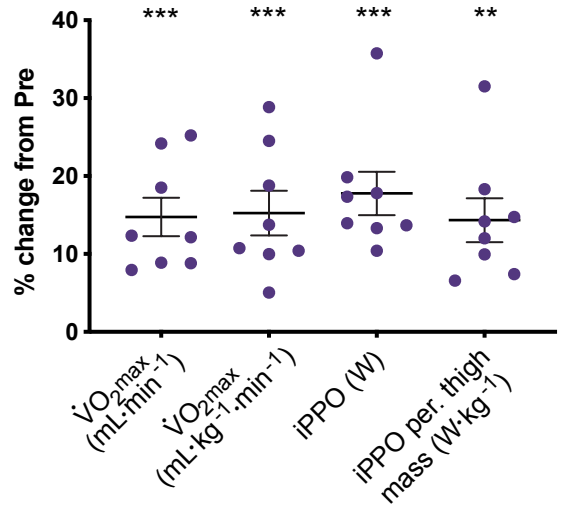


D

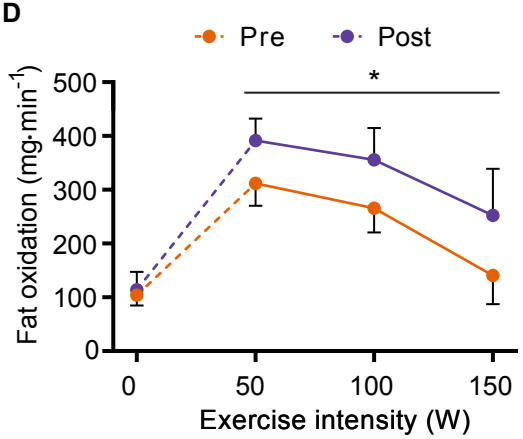


E

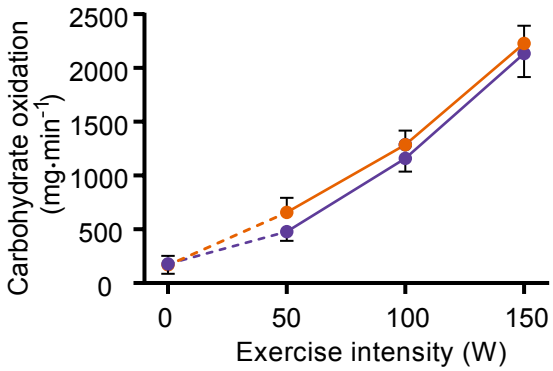


F

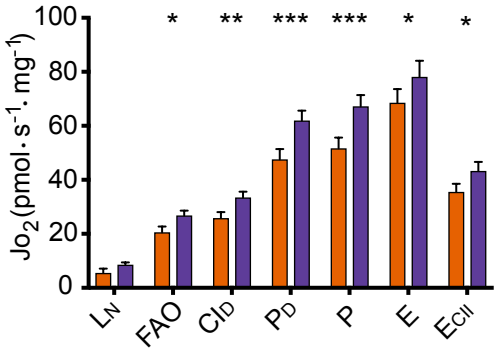


G

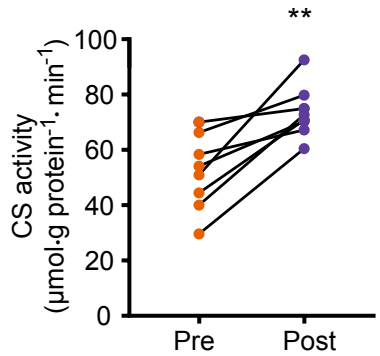


H

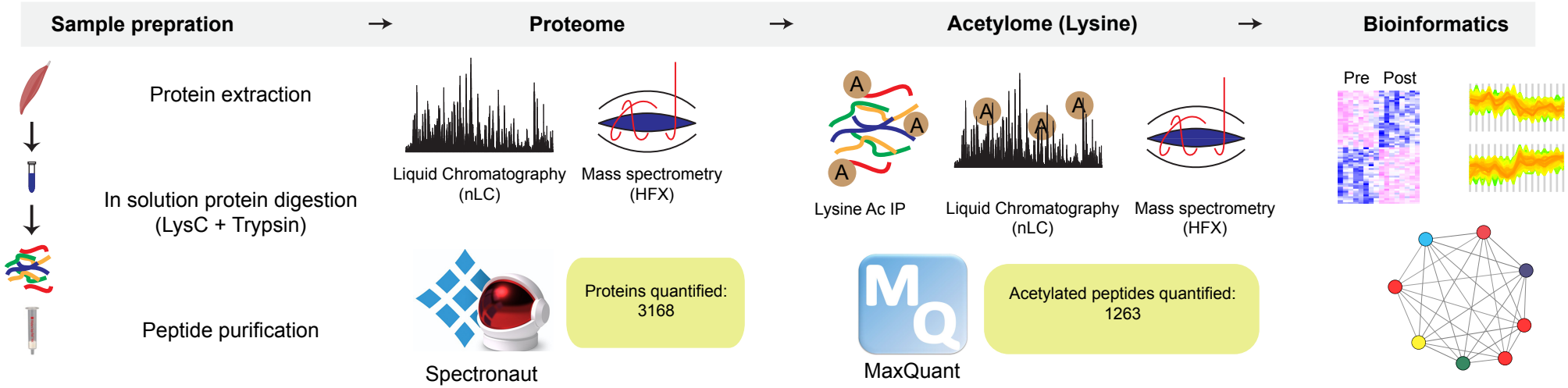

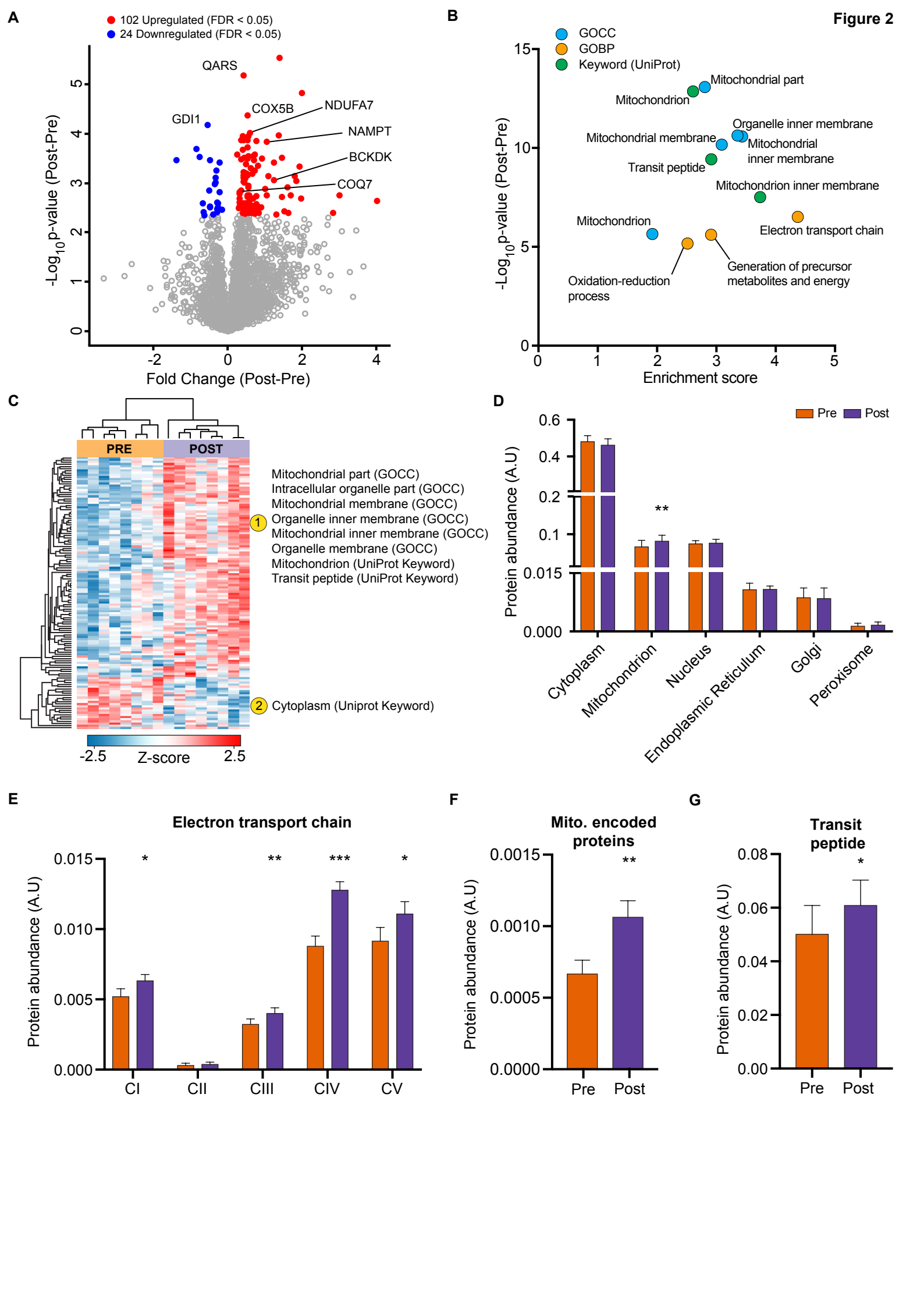
Figure 2
A
102 Upregulated (FDR < 0.05)
24 Downregulated (FDR < 0.05)
QARS
COX5B
NDUFA7
GDI1
NAMPT
BCKDK
COQ7
-Log10 p-value (Post-Pre)
Fold Change (Post-Pre)
B
GOCC
GOBP
Keyword (UniProt)
Mitochondrial part
Mitochondrion
Organelle inner membrane
Mitochondrial membrane
Mitochondrial inner membrane
Transit peptide
Mitochondrion inner membrane
Electron transport chain
Mitochondrion
Generation of precursor metabolites and energy
Oxidation-reduction process
-Log10 p-value (Post-Pre)
Enrichment score
C
PRE
POST
Mitochondrial part (GOCC)
Intracellular organelle part (GOCC)
Mitochondrial membrane (GOCC)
1 Organelle inner membrane (GOCC)
Mitochondrial inner membrane (GOCC)
Organelle membrane (GOCC)
Mitochondrion (UniProt Keyword)
Transit peptide (UniProt Keyword)
2 Cytoplasm (Uniprot Keyword)
-2.5
Z-score
2.5
D
Pre
Post
Protein abundance (A.U)
Cytoplasm
Mitochondrion
Nucleus
Endoplasmic Reticulum
Golgi
Peroxisome
E
Electron transport chain
Protein abundance (A.U)
CI
CII
CIII
CIV
CV
F
Mito. encoded proteins
Protein abundance (A.U)
Pre
Post
G
Transit peptide
Protein abundance (A.U)
Pre
Post

Figure 3

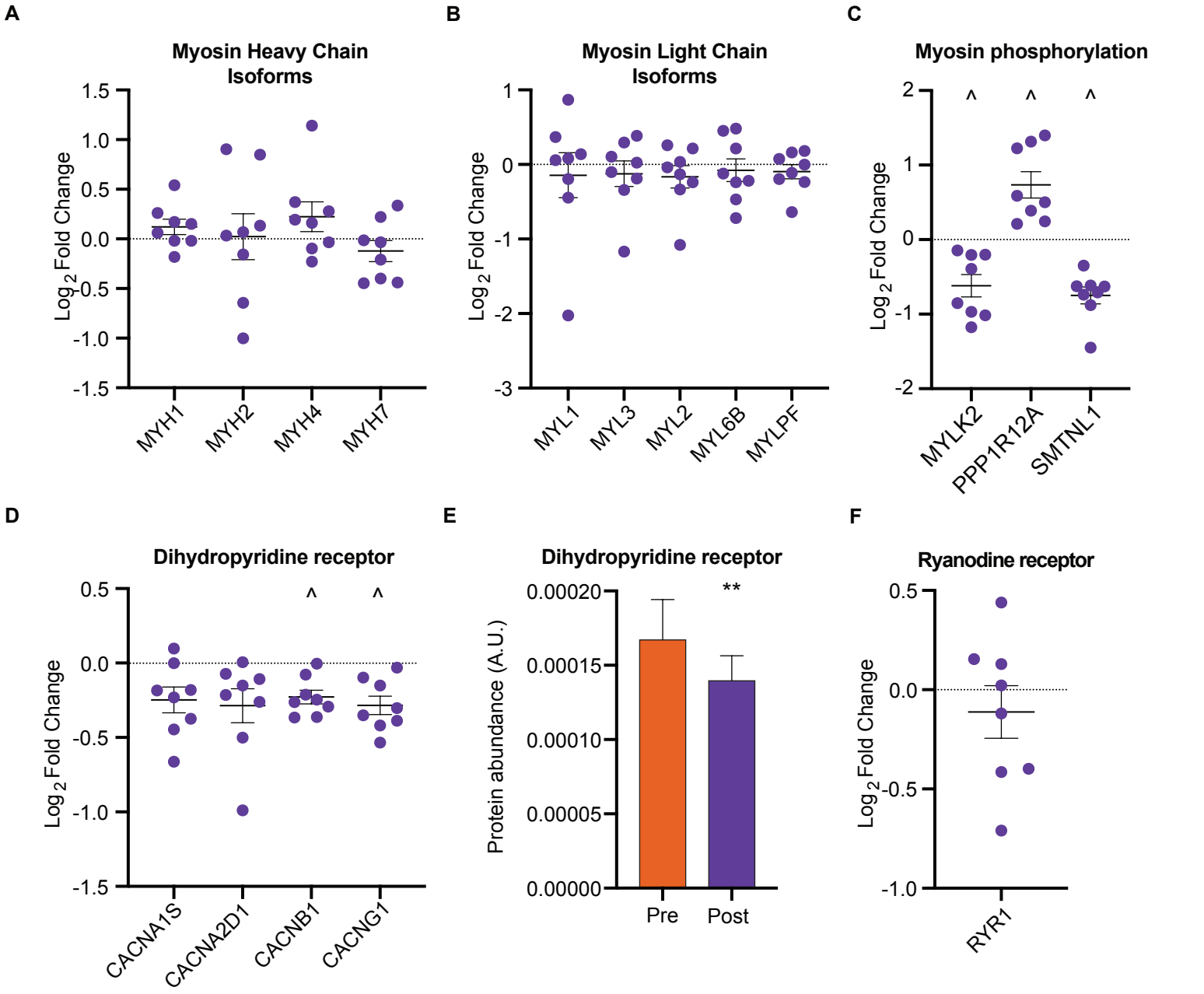
A
Myosin Heavy Chain Isoforms
Log2 Fold Change
1.5
1.0
0.5
0.0
-0.5
-1.0
-1.5
MYH1
MYH2
MYH4
MYH7
B
Myosin Light Chain Isoforms
Log2 Fold Change
1
0
-1
-2
-3
MYL1
MYL3
MYL2
MYL6B
MYLPF
C
Myosin phosphorylation
Log2 Fold Change
2
1
0
-1
-2
^
^
^
MYLK2
PPP1R12A
SMTNL1
D
Dihydropyridine receptor
Log2 Fold Change
0.5
0.0
-0.5
-1.0
-1.5
^
^
CACNA1S
CACNA2D1
CACNB1
CACNG1
E
Dihydropyridine receptor
Protein abundance (A.U.)
0.00020
0.00015
0.00010
0.00005
0.00000
**
Pre
Post
F
Ryanodine receptor
Log2 Fold Change
0.5
0.0
-0.5
-1.0
RYR1

Figure 4

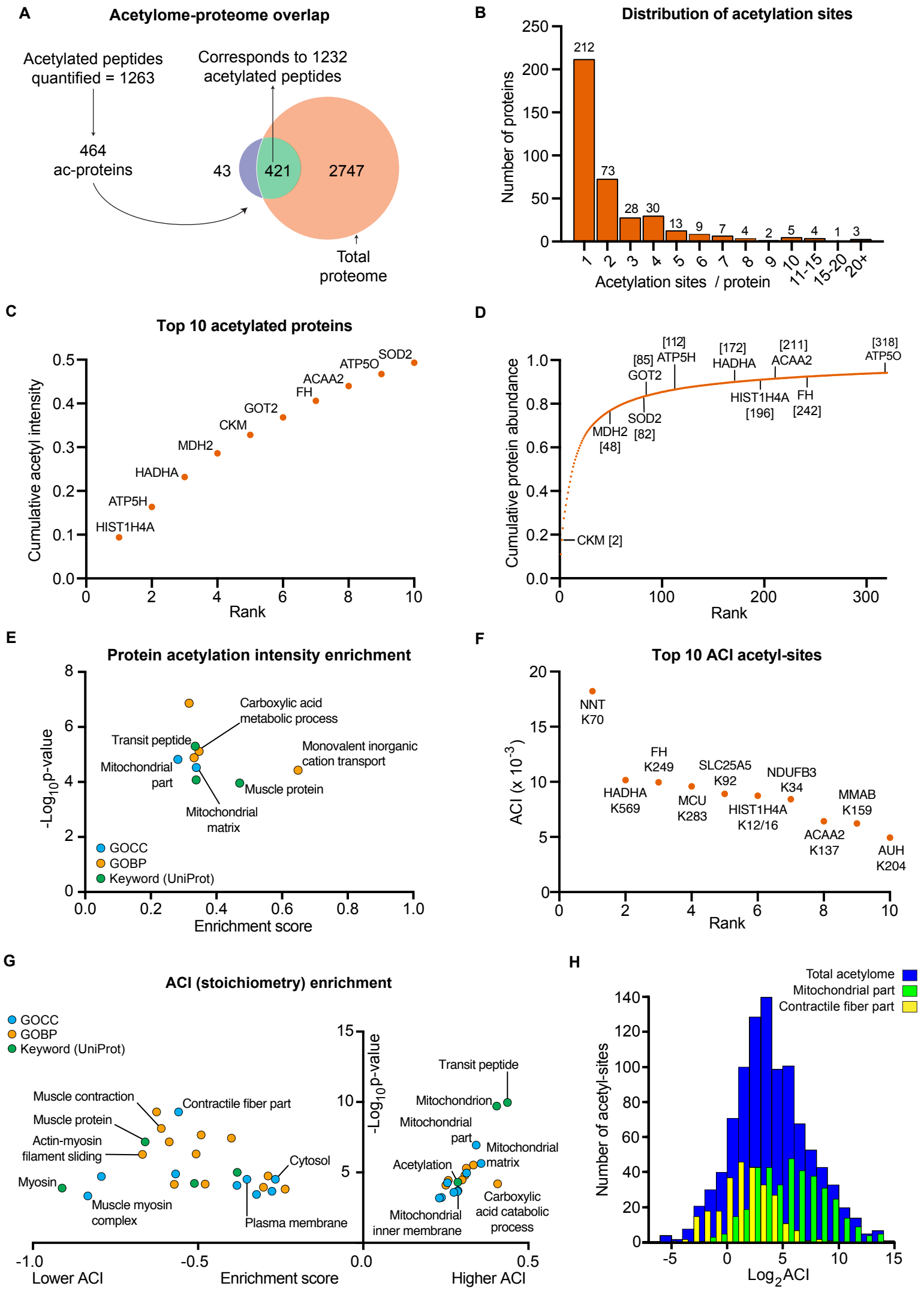
A
Acetylome-proteome overlap
Acetylated peptides quantified = 1263
464 ac-proteins
Corresponds to 1232 acetylated peptides
43
421
2747
Total proteome
B
Distribution of acetylation sites
Number of proteins
Acetylation sites / protein
212
73
28
30
13
9
7
4
2
5
4
1
3
1
2
3
4
5
6
7
8
9
10
11-15
15-20
20+
C
Top 10 acetylated proteins
Cumulative acetyl intensity
Rank
SOD2
ATP5O
ACAA2
FH
GOT2
CKM
MDH2
HADHA
ATP5H
HIST1H4A
D
Cumulative protein abundance
Rank
[318] ATP5O
[211] ACAA2
[172] HADHA
[112] ATP5H
[85] GOT2
HIST1H4A [196]
FH [242]
SOD2 [82]
MDH2 [48]
CKM [2]
E
Protein acetylation intensity enrichment
-Log10p-value
Enrichment score
Carboxylic acid metabolic process
Transit peptide
Monovalent inorganic cation transport
Mitochondrial part
Muscle protein
Mitochondrial matrix
GOCC
GOBP
Keyword (UniProt)
F
Top 10 ACI acetyl-sites
ACI (x 10-3)
Rank
NNT K70
FH K249
SLC25A5 K92
NDUFB3 K34
HADHA K569
MCU K283
HIST1H4A K12/16
MMAB K159
ACAA2 K137
AUH K204
G
ACI (stoichiometry) enrichment
GOCC
GOBP
Keyword (UniProt)
-Log10p-value
Muscle contraction
Contractile fiber part
Muscle protein
Actin-myosin filament sliding
Myosin
Muscle myosin complex
Cytosol
Plasma membrane
Transit peptide
Mitochondrion
Mitochondrial part
Mitochondrial matrix
Acetylation
Carboxylic acid catabolic process
Mitochondrial inner membrane
Lower ACI
Enrichment score
Higher ACI
H
Total acetylome
Mitochondrial part
Contractile fiber part
Number of acetyl-sites
Log2ACI

Figure 5

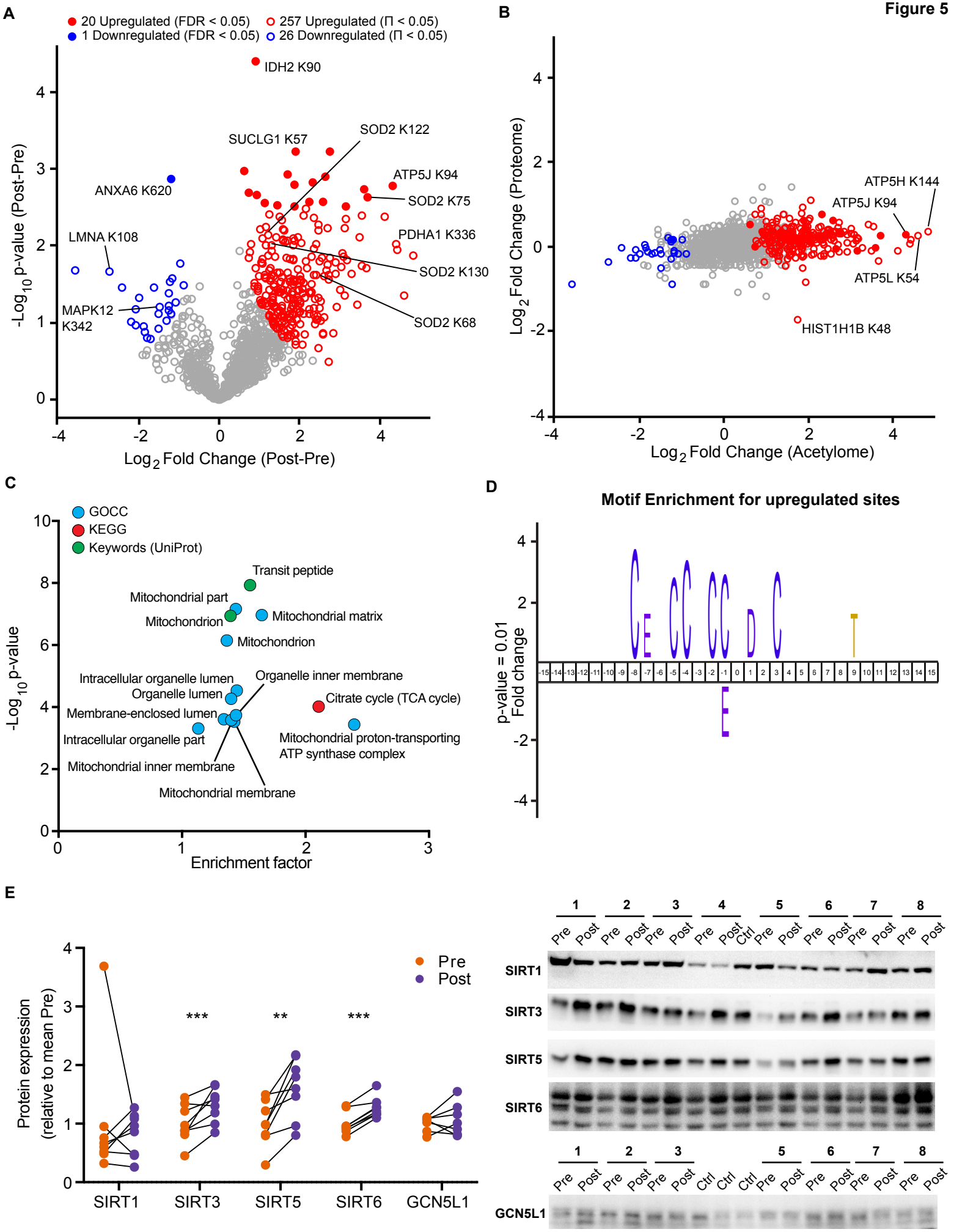
A
20 Upregulated (FDR < 0.05)
257 Upregulated (Π < 0.05)
1 Downregulated (FDR < 0.05)
26 Downregulated (Π < 0.05)
IDH2 K90
SUCLG1 K57
SOD2 K122
ATP5J K94
SOD2 K75
ANXA6 K620
PDHA1 K336
LMNA K108
SOD2 K130
MAPK12 K342
SOD2 K68
-Log10 p-value (Post-Pre)
Log2 Fold Change (Post-Pre)
B
ATP5H K144
ATP5J K94
ATP5L K54
HIST1H1B K48
Log2 Fold Change (Proteome)
Log2 Fold Change (Acetylome)
C
GOCC
KEGG
Keywords (UniProt)
Transit peptide
Mitochondrial part
Mitochondrion
Mitochondrial matrix
Mitochondrion
Intracellular organelle lumen
Organelle inner membrane
Organelle lumen
Citrate cycle (TCA cycle)
Membrane-enclosed lumen
Intracellular organelle part
Mitochondrial proton-transporting ATP synthase complex
Mitochondrial inner membrane
Mitochondrial membrane
-Log10 p-value
Enrichment factor
D
Motif Enrichment for upregulated sites
p-value = 0.01
Fold change
E
Pre
Post
Protein expression (relative to mean Pre)
SIRT1
SIRT3
SIRT5
SIRT6
GCN5L1
Ctrl

Figure 6

A

**Protein:**

Log$_2$ fold change (protein)

-2 2

Undetected

**Acetylation site:**

- Upregulated (Π < 0.05)
- Downregulated (Π < 0.05)
- Unchanged (Π > 0.05)

NDUFAB1, NDUFA9, NDUFA10, NDUFV1, NDUFA2, NDUFV2, NDUFB9, NDUFV3, NDUFA7, NDUFB6, NDUFS5, NDUFS6, NDUFS1, NDUFA5, NDUFB3

SDHA, SDHB

MT-ATP8, ATP5H, ATP5B, ATP5O, ATP5C1, ATP5J, ATP5D, ATP5L, ATP5F1, ATP5A1, ATPIF1, ATP5E

CI, CII, CIII, CIV, CV

UQCRC2, CYC1, UQCRB, UQCRH, UQCRC1

COX4I1, COX6B1, COX5B

B

Pyruvate

PDHX, PDHA1, DLAT

Acetyl CoA

CS

Oxaloacetate

Citrate

ACO2

MDH1, MDH2

Malate

Isocitrate

IDH3A, IDH1, IDH3B, IDH2

FH

TCA Cycle

Fumarate

2-oxogluterate

SDHA, SDHB

OGDH, DLST

Succinate

SUCLG2, SUCLG1, DLD

Succinyl CoA

SUCLA2

C

ACTC1, MYH4, MYBPC1, ACTN2

MYL1, MYH3, MYL2, TNNT1, TNNI1

MYH7, MYH9, TPM2, NEB

ACTN3, DMD, MYH1, TTN

TPM4

VIM

TNNT3, TNNI2, MYL3, DES

MYH2, TPM1, TPM3, MYBPC2

Figure 7

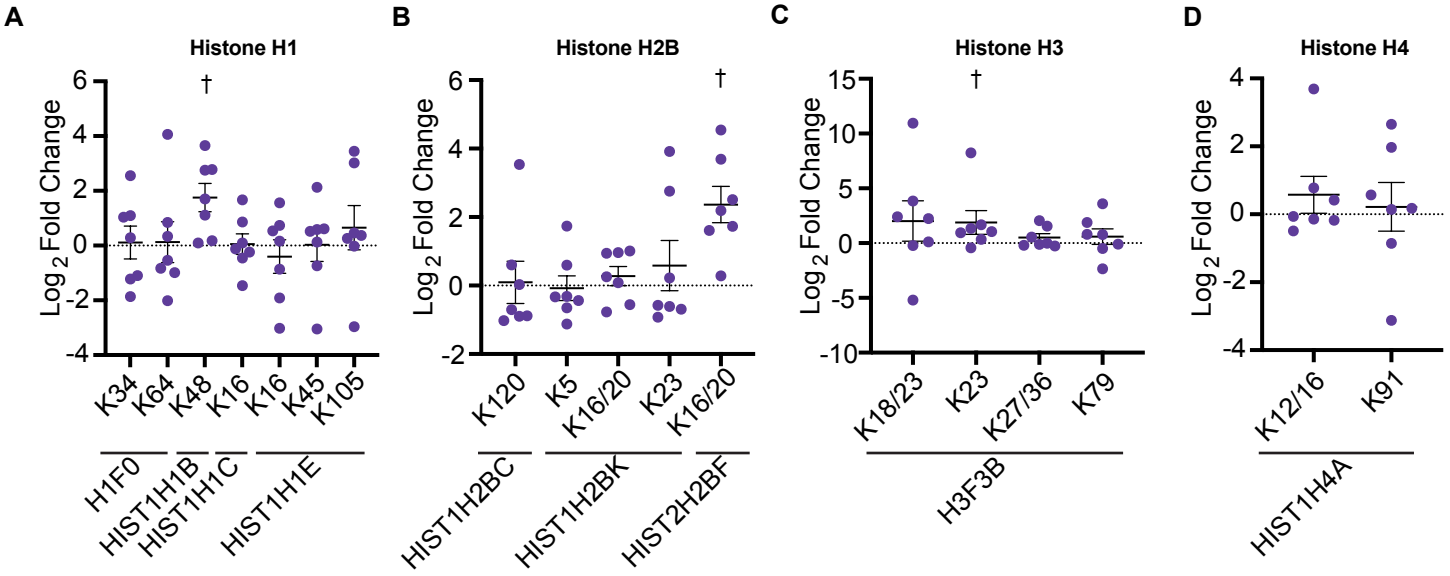
A
Histone H1
Log2 Fold Change
K34
K64
K48
K16
K16
K45
K105
H1F0
HIST1H1B
HIST1H1C
HIST1H1E
B
Histone H2B
K120
K5
K16/20
K23
K16/20
HIST1H2BC
HIST1H2BK
HIST2H2BF
C
Histone H3
K18/23
K23
K27/36
K79
H3F3B
D
Histone H4
K12/16
K91
HIST1H4A

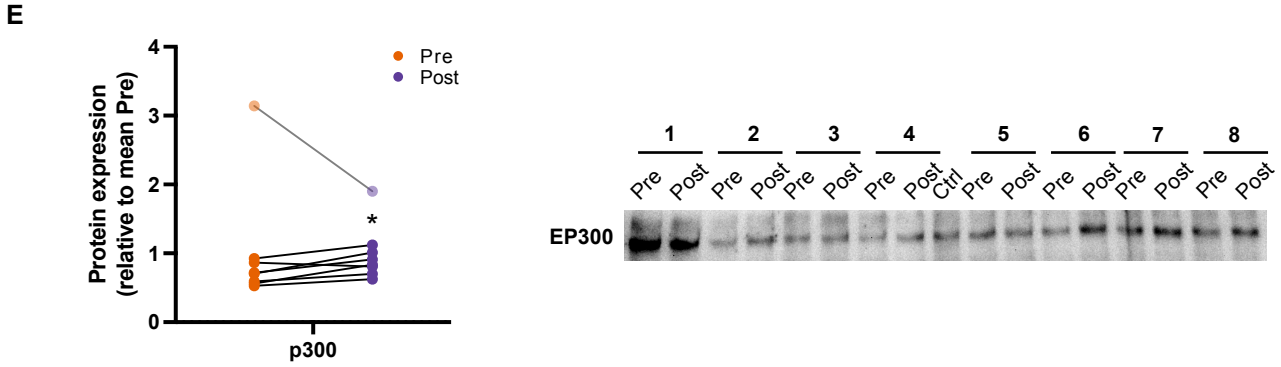
E
Protein expression (relative to mean Pre)
Pre
Post
p300
1
2
3
4
5
6
7
8
Pre
Post
Ctrl
EP300

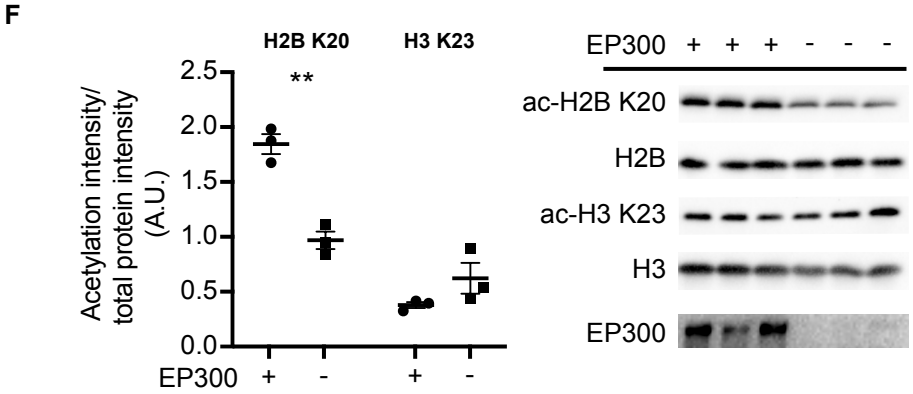
F
H2B K20
H3 K23
Acetylation intensity/ total protein intensity (A.U.)
EP300
ac-H2B K20
H2B
ac-H3 K23
H3
EP300